Parallel Synthesis and Screening of Supramolecular Chemosensors that Achieve Fluorescent Turn-On Detection of Drugs in Saliva

Meagan A. Beatty, Allison J. Selinger, YuQi Li, and Fraser Hof*

Department of Chemistry, University of Victoria, PO Box 3065, STN CSC, Victoria, V8W 3V6, Canada.
E-mail: fhof@uvic.ca

ABSTRACT

Programming and controlling molecular recognition in aqueous solutions is increasingly common, but creating supramolecular sensors that detect analytes in biologically relevant solutions remains a non-trivial task. We report here a parallel synthesis-driven approach to create a family of self-assembling dimeric sensors that we call DimerDyes, and its use for the rapid identification of salt-tolerant sensors for illicit drugs. We developed an efficient method that involves parallel synthesis and screening in crude form without the need to purify each potential sensor. Structurally diverse "hit" DimerDyes were re-synthesized, purified and were each shown to assemble into homodimers in water in the programmed way. DimerDyes provided a "turn-on" fluorescence detection of multiple illicit drugs at low micromolar concentrations in water and in saliva. The combination of multiple agents into a sensor array was successfully able to detect and discriminate between closely related drugs and metabolites in multiple important drug families.

INTRODUCTION

Supramolecular sensors, once limited to organic solvents and aqueous/organic mixtures, can now detect biologically relevant analytes even in salty aqueous solutions.[1-9] Analyte detection in water is made more difficult and less predictable when the target is found in complex biological media. Examples of supramolecular sensing in human cells,[10-14] enzyme-supporting buffers,[15-21] bacterial culture,[22] and real biofluids[23-26] now exist, but the *de novo* design of new sensing systems that work in complex biological media remains non-trivial.

We recently reported a novel chemosensor, DimerDye 1 (**DD1**), that operates via an inherently salt-tolerant supramolecular sensing mechanism. The sensor contains a styryl-type merocyanine dye synthetically integrated into the calix[4]arene macrocycle.[15] In water, the topology of **DD1** leads to self-assembly in water into a non-emissive homodimer. Upon the addition of methyllysine-containing peptides that are good guests, the dimer disassembles and forms a fluorescent DimerDye-methyllysine complex (Figure 1a). We showed that **DD1** was able to monitor the enzymatic methylation and demethylation of peptides in real-time. Due to the intrinsic salt tolerance of this molecular design, the sensor operated in the presence of high concentrations of NaCl, reducing agents, transition metal salts, and other enzyme co-factors.[27]

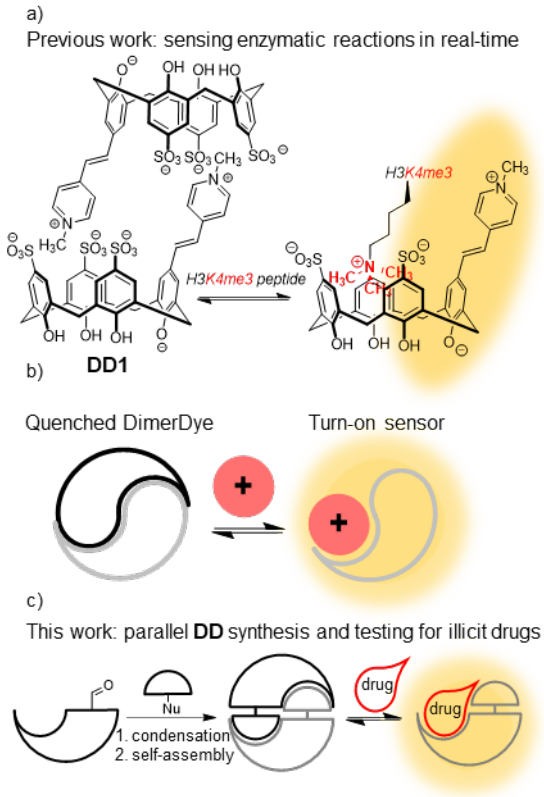

Figure 1. a) Previous work: **DD1** can monitor an enzymatic reaction that produces a trimethyllysine-containing peptide that is bound and detected by **DD1**. b) A cartoon illustrates the guest-induced disassembly and sensing mechanism of the self-assembled DimerDye. c) This work reports the development of a parallel synthesis and screening of diverse new DimerDyes (DDs) to detect cationic drugs in biological media.

Parallel synthesis can give rapid access to sensor molecules. It provides a means to create many products in a quick and combinatorial fashion, and to screen a broad structural space without needing atom-by-atom design. Sensors created by parallel synthesis approaches have typically been inorganic or polymer-based,[28-30] while relatively few examples of discrete organic sensing molecules have been generated in this way.[31-34] One example of particular interest involved the condensation of a set of aromatic aldehydes with a set of heterocyclic nucleophiles to form 276 fluorescent styryl dyes.[35] The reaction mixtures were tested directly in cells for organelle accumulation and 119 dyes were identified as responsive sensors, although no particular sensing mechanism or analyte binding functions had been included in the library design. This approach was attractive to us as the chromophores in the library resembled those of our styryl-based DimerDye.

We report here a parallel synthesis-driven approach to creating new DimerDyes, and its use in a pilot study that rapidly identifies sensors for illicit drugs. Many classes of drugs, including opioids, amphetamines, tropane alkaloids, and anaesthetics, contain a hydrophobic cation in their structure that we hypothesized would be recognized by sulfonatocalix[4]arene-based hosts. Since **DD1**[15] and other related molecules[27, 36-37] can assemble and/or bind guests in competitive aqueous buffers, we envisioned that this property could be extended to sensing drugs in biofluids. Unlike most supramolecular host-guest projects, we eschewed the atomic design of sensors that would be highly specific for individual drug molecules. Instead, we developed a parallel synthesis and efficient crude screening process to quickly identify new sensors for the detection of a given analyte in a given solution. We also report the re-synthesis, detailed characterization of sensing mechanisms and limits of detection for a set of structurally diverse "hit" DimerDyes that arose from our screen. To demonstrate the broad scope of this new approach, we describe a sensor array that can identify members of multiple classes of illicit drugs.

RESULTS

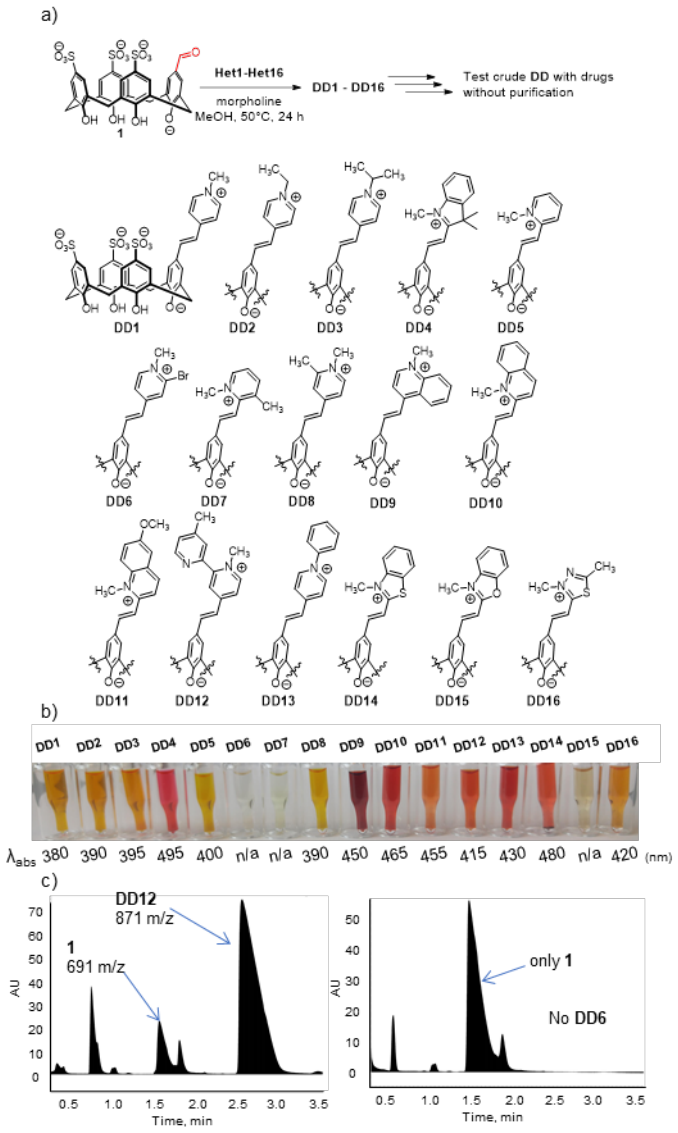

Figure 2. Parallel synthesis provides a library of DimerDye chemosensors. a) Condensation reactions with aldehyde-bearing calix[4]arene, **1**, and **Het1–16** give DimerDyes, **DD1–DD16**. b) Aliquots of crude reaction mixtures show the characteristic colour changes that we use as a visual sign of reaction success for 13 out of 16 DimerDyes after heating mixture at 50°C in methanol for 6 hours. c) Two exemplary traces, showing UPLC-MS data for a successful synthesis (**DD12**) and a failed synthesis (**DD6**). See Supporting information for full UPLC-MS data of all runs.

We first developed an efficient method for the parallel synthesis of new DimerDyes. We anticipated that varying the fluorophore on the edge of the binding pocket would create DDs with diverse homodimerization affinities and guest-binding selectivities, but that would retain the

general features of disassembly-driven molecular sensing and salt tolerance that were found in the parent molecule **DD1**. We selected 16 heterocyclic nucleophiles (**Het1–16**) that form merocyanine fluorophores after condensation with the aldehyde precursor, **1** (Figure 2a). Our previous synthesis of DimerDyes involved heating at reflux **1** and **Het1** with piperidine in methanol overnight.[15] We quickly found that the protonated piperidinium by-product is itself a good guest that interferes with sensor screening. Instead, morpholine was selected as an amine-containing base as its high hydrophilicity would minimize complexation with the hydrophobic binding pockets. Successful condensation reactions are indicated by a colour change after 6 hours at 50°C (Figure 2b). UPLC-MS confirms product formation and reveals the extent of each reaction (Figure 2c and Supporting Information). 13 of the 16 DimerDye syntheses go to full or partial completion, while syntheses of **DD6**, **DD7**, and **DD15** fail under the listed conditions.

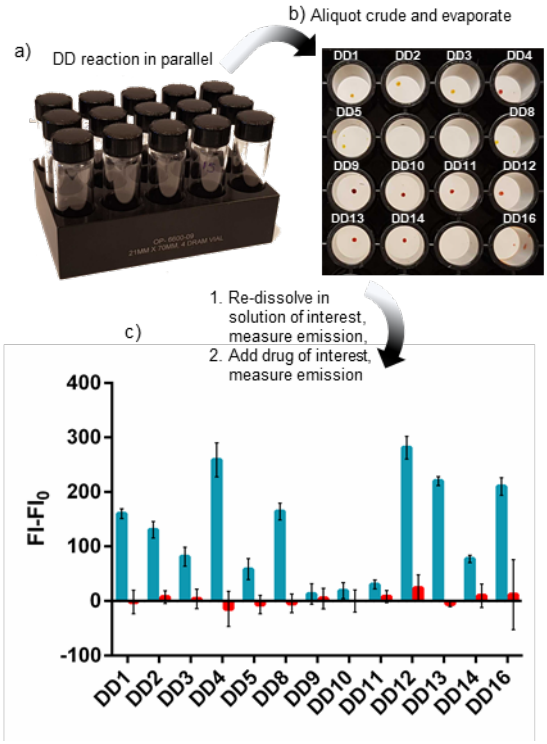

Figure 3. Scheme of parallel DimerDye synthesis and crude screening for nicotine and acetaminophen. a) Each DimerDye reaction occurs in a separate vial, heated in an aluminium block. b) The crude mixture is aliquoted to a black-walled 96-well plate and evaporated. c) The pellets are re-dissolved in buffered water and initial fluorescence is measured. The analyte of interest is added, fluorescence is measured again and the difference in fluorescence is determined. Blue bars = 10 μM nicotine, red bars = 10 μM acetaminophen. See Supporting Information for excitation and emission wavelengths used.

A rapid, crude screening process successfully identified DimerDye sensors without first needing to purify each compound. The crude reactions were directly aliquoted into 96-well plates and the reaction solvent was allowed to evaporate (Figure 3a and 3b). The dried pellets were re-suspended in sodium phosphate buffer (10 mM, pH 7.4). Nicotine was added as a model analyte. The increases in fluorescence in certain wells indicate the creation of good nicotine sensors. To confirm that the fluorescence change arises from host-guest binding, we counter-screened the library against acetaminophen, which is neutral and should not bind DimerDyes. Acetaminophen generates little to no fluorescence in all cases (Figure 3c).

We selected a subset of structurally diverse sensors for follow-up mechanistic studies. From the fluorescence responses to nicotine, we selected **DD1**, **DD4**, **DD8**, **DD12**, and **DD13** as active sensors to re-synthesize, purify and study. We also selected an inactive sensor, **DD9**, so we could learn more about the parallel synthesis and screening results.

Each of the selected DimerDyes assembled into homodimers in water in the programmed way, regardless of the structure of the pendant groups. Selected sensors were obtained with modest yields (23–55%) after re-synthesis and purification by reverse-phase HPLC. ^{1}H NMR spectra confirm each sensor exist as homodimers when dissolved in buffered-D_2O. The signature feature of homodimerization is upfield shift and broadening of pendant group resonances due to encapsulation in the electron-rich calix[4]arene pocket. Aromatic resonances in the selected sensors shifted upfield by 1.23-3.69 ppm, while aliphatic (methyl) resonances shifted upfield by 0.46-3.60 ppm (Table S1), compared to the shifts observed for the parent heterocycles. In all cases the protons farthest out on the pendant arm had the greatest upfield shifts. This indicates those protons are the most deeply buried in the pocket of the opposing calixarene in each dimer. 1D DOSY NMR on **DD4** confirmed that its hydrodynamic radius was typical for a dimeric assembly and larger than the non-dimerizing aldehyde precursor, **1** (Tables 1, S3, and S5). Interestingly, inactive sensor **DD9** also shows clear signs of dimerization with the *N*-CH_3 and ortho-proton shifted 2.50 ppm and 2.61 ppm, respectively.

Table 1. 1D DOSY obtained diffusion coefficients and hydrodynamic radii of **1**, **DD4** alone and **DD4** complexed to nicotine

	Diffusion Coefficient, m^2/s	r_H, Å
1	3.31×10^{-10}	7.63 ± 0.02
DD4	1.97×10^{-10}	12.47 ± 0.15
DD4 + 20 eq. nicotine	2.52×10^{-10}	9.74 ± 0.21

The fluorescence responses arise from the disassembly of each DimerDye and host-guest complexation with analyte. ^{1}H NMR titrations of nicotine into each DimerDye show resonances broadening partially or completely, indicating dimer disassembly and nicotine complexation at an intermediate timescale relative to NMR. Nicotine titrations into **DD4** and **DD12** most clearly show the host resonances returning from upfield-shifted locations and/or broadening (Figure 4a and Supporting Information). **DD4** resonances stay sharp enough in the presence of 20 eq. nicotine to conduct 1D DOSY experiments, and as expected the hydrodynamic radius of **DD4** decreases to a value expected for a monomeric calixarene-nicotine complex (Tables 1 and S4). Comparing the NMR tubes before and after the addition of nicotine shows visible DD fluorescence only for the nicotine-containing samples when irradiated at 365 nm with a hand-held UV lamp (Figures 4b and S16). This behavior is further confirmed with titrations of nicotine into **DD12** monitored by fluorescence spectroscopy. The dimer alone is barely fluorescent when irradiated at 415 nm, but upon addition of nicotine the fluorescence emission at 640 nm increases (Figure 4c and Supporting Information). This turn-on fluorescence response is observed by all selected DimerDyes except for **DD9**, which shows nicotine complexation by NMR yet remains dark when irradiated with the UV hand-held lamp and when studied on a fluorescence spectrometer.

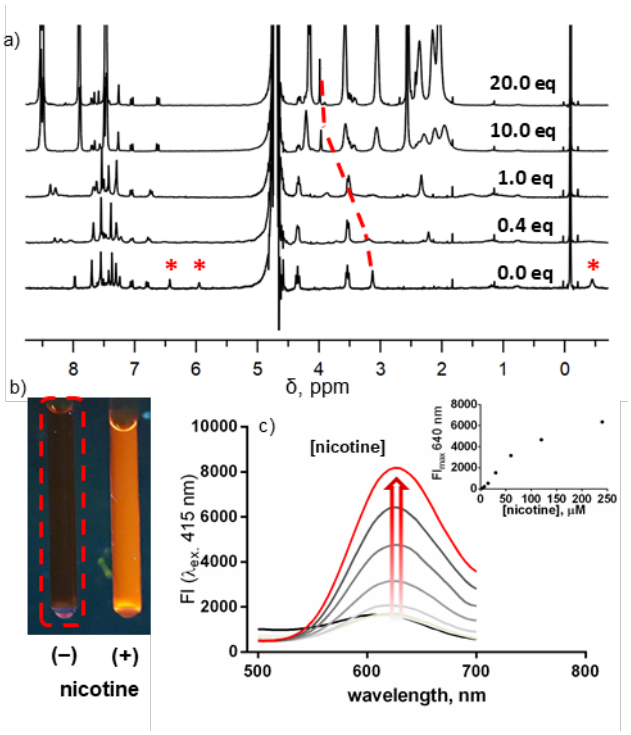

Figure 4. Nicotine titrations reveal disassembly of dimer and formation of fluorescent DD–nicotine complex. a) ^{1}H NMR titrations of nicotine into **DD12** (500 μM) show fluorophore resonances in either fast exchange by shifting downfield (red dotted lines) or in intermediate exchange and broadening (red stars) indicative of disassembly and formation of a nicotine host-guest complex. b) Picture of NMR tubes with **DD12** without nicotine (–) or with nicotine (+) when irradiated by a hand-held UV lamp. c) Fluorescence titrations of nicotine into **DD12** (12 μM) shows a dose-dependent increase in fluorescence. The red trace indicates [nicotine] = 240 μM, while black line indicates no nicotine present. All samples are in NaH_2PO_4/Na_2HPO_4 (10 mM, pH 7.4) buffer.

DimerDyes provide turn-on fluorescence detection of different drugs at low micromolar concentrations in water and in saliva. Three exemplary drugs were chosen from different drug classes: nicotine, methylenedioxymethamphetamine (Ecstasy, or MDMA), and cocaine. In both water and saliva, all five selected DimerDyes detect all three drugs at low μM concentrations (Table S6 and S7). **DD8** detects nicotine in water and in saliva with limits of detection at 3.4 μM and 18.6 μM, respectively (Figure 5a and b). Even MDMA, a secondary amine and therefore a weaker guest, induces a response from **DD1** in both water and saliva with limits of detection at 2.7 μM and 41.2 μM, respectively (Figure 5c and d). **DD13** detects cocaine equally well in buffer and in saliva, with limits of detection of 2.7 μM in both fluids (Figure 5e and f).

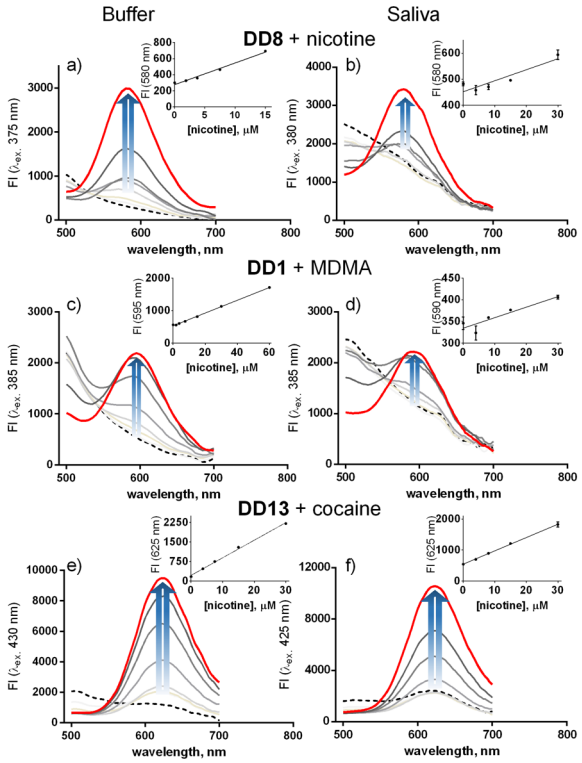

Figure 5. Exemplary fluorescence titrations of different drugs into DimerDyes in buffered water and saliva. Nicotine titrations into **DD8** in a) buffered water and in b) saliva. MDMA titrations into **DD1** in c) buffered water and in d) saliva. Cocaine titrations into **DD13** in e) buffered water and in f) saliva. [**DD**] = 12 µM, red bold trace indicates [drug] = 240 µM, dashed black line indicates no drug present. "Buffer" is NaH_2PO_4/Na_2HPO_4 (10 mM, pH 7.4) and "Saliva" is a 1:1 dilution of saliva with water; dilution is necessary to allow for accurate, bubble-free pipetting of saliva. See Supporting Information for the complete set of titrations.

We next explored the combination of multiple agents into a sensor array. This approach has distinct advantages over the use of single sensors designed for individual analytes. Often chemosensors cross-detect many analytes that are present in a complex mixture. Instead of re-designing a chemosensor to improve selectivity, the original system can be expanded to form an array of chemosensors that cross-react with many analytes but to different extents. This complex output is a unique fingerprint for each analyte. Multivariate analysis, including methods like principal component analysis (PCA) and linear discriminant analysis (LDA), can analyze the 'fingerprints' by both reducing the dimensionality of the data and creating a useful way to represent the differential responses. Anslyn *et al.* first developed these techniques for a wide variation of applications, including sensor arrays that can differentiate flavonoids in wine[38] and

those that can classify different cancer cells.[39] Others have used supramolecular array sensors to differentiate chemical marks on histone proteins,[40-41] different anions in toothpaste,[42] and protein recognition from pattern-generating multi-dye probes.[43]

A sensor array of five DimerDyes was successfully able to detect and discriminate between closely related drugs and metabolites in multiple drug families. We studied amphetamines, opiates, and alkaloids, and included nicotine and acetaminophen alongside each different drug family as these two drugs are commonly found in individuals. Figure 6a shows that the active drugs, MDMA and methamphetamine (MA), are discriminated from their respective metabolites, methylenedioxyamphetamine (MDA) and amphetamine (A), even though each differs from its metabolite by only a single methyl group. The array in Figure 6b also differentiated between cocaine, its main metabolite benzoylecgonine, as well as lidocaine and procaine, which are common adulterants found in illegally purchased cocaine.[44] Figure 6c shows a 3D score plot that highlights the discrimination between heroin and its metabolite 6-monoacetylmorphine (6-MAM), while oxycodone and oxymorphone are not perfectly discriminated as both clusters of replicate data are nearly overlapping.

DimerDyes can function individually or as an array of sensors. Each sensor cross-reacted as expected with each drug, but the uniqueness of the generated fluorescence fingerprint was sometimes limited.[45] This is highlighted by the low variance (< 5%) along the second principal component (F2) in the amphetamines and anaesthetics class. This suggests that in some settings DimerDyes might be able to operate independently and not necessarily within an array. The benefit of the DD array is the easy visualization of the data for drug identification. It is easier to map combinations of drugs with common adulterants or their metabolites by the PCA score plots rather than fluorescence bar graphs (Figure S32).

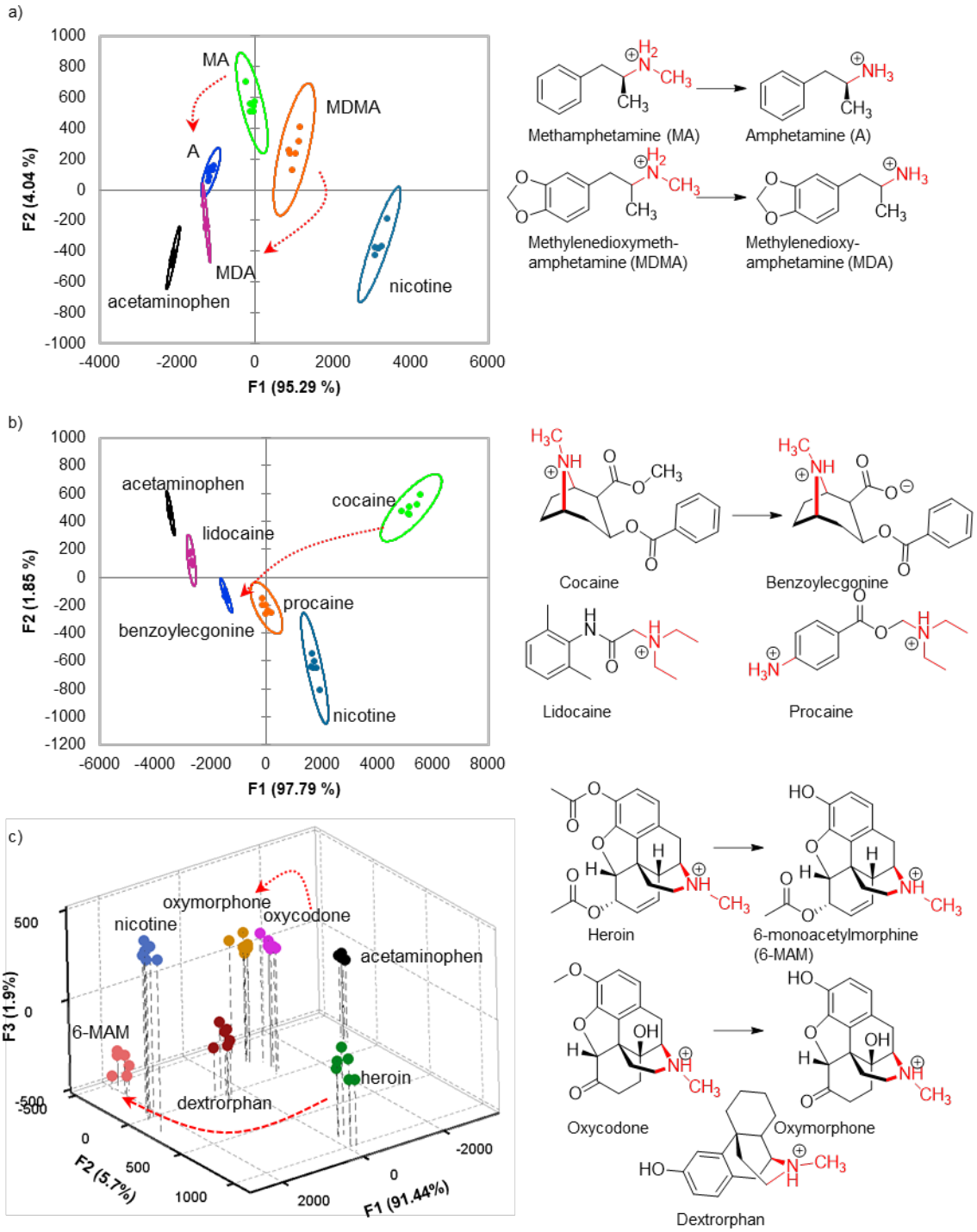

Figure 6. Principal component analysis (PCA) score plots distinguish between different members and classes of drugs by five DimerDye sensors (**DD1**, **DD4**, **DD8**, **DD12**, **DD13**) operating within an array. a) PCA plot of amphetamines are well discriminated with samples clustered and separated from each other. b) PCA plot of anaesthetics c) 3D PCA plot of opioids. Red dotted lines map the parent drug to its main metabolite. Structures in each class are shown to the right. Red motifs are recognized by the calixarene pocket. Each sample cluster is enclosed by 95%

confidence ellipses. [DD] = 12 μM, [drug] = 100 μM and in a NaH_2PO_4/Na_2HPO_4 (10 mM, pH 7.4) buffer.

DISCUSSION

The final, parallel synthetic step described here gives access to new agents with a common sensing mechanism, but with varying photophysical properties and guest-binding properties. The successful structures included merocyanines based on *N*-methylpyridinium (**DD1** and **DD8**), indolinium (**DD4**), bipyridinium (**DD12**) and *N*-phenylpyridinium (**DD13**). The new **DD** sensors have tunable excitation and emission wavelengths (λ_{exc} 380-475 nm, λ_{em} 570-640 nm), with Stokes shifts between 95 nm and 215 nm. The variable structures in this small DimerDye library also translated into different binding properties for different drugs. The quinolinium dyes, **DD9** – **DD11**, were not as guest-responsive due to an unpredicted photophysical deficiency rather than poor self-dimerization or guest recognition. This highlights the strength of the parallel synthesis and crude screening process, as it would allow us going forward to avoid the wasted effort in synthesizing, purifying, and characterizing a sensor only to find that it is inoperative for an unknown reason.

These new supramolecular agents have sensitivities in real biological solutions that meet or approach the values seen in real human samples. DimerDyes remain functional in saliva that often contains 3 g/L of proteins and 20 – 100 mM concentrations of various salts.[46] To our knowledge, there are only a few supramolecular chemosensors that operate in biofluids, like urine, which reflects the difficulty of working in such medium.[23-24, 47] Drug concentrations in saliva reach low μM within an hour of consumption and we have shown that our DimerDye sensors can detect at or near these concentrations.[48-52] For example, MDMA concentrations reach 35 μM in saliva 1.5 hours after consumption,[48] while cocaine can be present in saliva at 1 μM after 2 hours.[49, 52]

The power of a sensor array to detect many analytes without the need for excellent specificity or rational design was demonstrated with the combination of five different DimerDyes (**DD1**, **DD4**, **DD8**, **DD12**, **DD13**). From our nicotine, MDMA, and cocaine titrations, we noticed that subtle changes in drug structure induced small but significant changes in

fluorescence responses. Those differences translated into substantial success when the **DD**s were deployed in a sensor array. The combination of our five sensors and PCA plots, we were able to reasonably distinguish between each member within a drug class. A jackknife analysis showed that we were also able to successfully classify 100% of members within the opioid and anaesthetics families, and to achieve 96% success in the amphetamines family (see Supporting Information).

CONCLUSION

This approach to developing new sensors is accessible, efficient and flexible. The parallel synthesis approach that we report here will be easily expanded upon, enabling the discovery of more DimerDye sensors that work for different cationic analytes, and that operate in different biological solution conditions. The promiscuity of sulfonated calixarenes, coupled with the general success of this approach in salty water, combine to suggest that this concept can be applied to many different cationic analytes in many different aqueous solutions. Expanding the diversity libraries using known synthetic approaches will generate a library of crude sensors that could be quickly tested for the ability to detect any given cationic analyte in its native biological fluid.[35] Furthermore, we envision that this parallel approach can be expanded to include other dye-appended macrocycles to identify sensors for a wider variety of biological analytes.

ASSOCIATED CONTENT

Supporting Information

The Supporting Information is available free of charge on the ACS Publications website.

Synthesis of novel compounds, NMR/UV-Vis/fluorescence characterization of assembly, parallel synthesis and testing optimization, fluorescence analyte detection, limits of detection, PCA and LDA protocols (PDF).

AUTHOR INFORMATION

Corresponding Author

*fhof@uvic.ca.

Notes

The authors declare no competing financial interests.

ACKNOWLEDGEMENTS

We thank the National Science and Engineering Research Council (NSERC, Discovery Grant #RGPIN-2019-04806) and Canada Research Chairs program for financial support.

REFERENCES

(1) Gale, P. A.; Caltagirone, C. Anion sensing by small molecules and molecular ensembles. *Chem. Soc. Rev.* **2015,** *44*, 4212-4227.

(2) You, L.; Zha, D.; Anslyn, E. V. Recent Advances in Supramolecular Analytical Chemistry Using Optical Sensing. *Chem. Rev.* **2015,** *115*, 7840-92.

(3) Ghale, G.; Nau, W. M. Dynamically Analyte-Responsive Macrocyclic Host–Fluorophore Systems. *Acc. Chem. Res.* **2014,** *47*, 2150-2159.

(4) Wu, D.; Sedgwick, A. C.; Gunnlaugsson, T.; Akkaya, E. U.; Yoon, J.; James, T. D. Fluorescent chemosensors: the past, present and future. *Chem. Soc. Rev.* **2017,** *46*, 7105-7123.

(5) Aryal, G. H.; Hunter, K. W.; Huang, L. A supramolecular red to near-infrared fluorescent probe for detection of drugs in urine. *Org. Biomol. Chem.* **2018**.

(6) Minami, T.; Esipenko, N. A.; Zhang, B.; Isaacs, L.; Anzenbacher, P. "Turn-on" fluorescent sensor array for basic amino acids in water. *Chem. Commun.* **2014,** *50*, 61-63.

(7) Gober, I. N.; Waters, M. L. Supramolecular Affinity Labeling of Histone Peptides Containing Trimethyllysine and Its Application to Histone Deacetylase Assays. *J. Am. Chem. Soc.* **2016,** *138*, 9452-9459.

(8) Gill, A. D.; Perez, L.; Salinas, I. N. Q.; Byers, S. R.; Liu, Y.; Hickey, B. L.; Zhong, W.; Hooley, R. J. Selective Array-Based Sensing of Anabolic Steroids in Aqueous Solution by Host–Guest Reporter Complexes. *Chem. Eur. J.* **2019,** *25*, 1740-1745.

(9) Kolusheva, S.; Zadmard, R.; Schrader, T.; Jelinek, R. Color Fingerprinting of Proteins by Calixarenes Embedded in Lipid/Polydiacetylene Vesicles. *J. Am. Chem. Soc.* **2006,** *128*, 13592-13598.

(10) Ghale, G.; Lanctôt, A. G.; Kreissl, H. T.; Jacob, M. H.; Weingart, H.; Winterhalter, M.; Nau, W. M. Chemosensing Ensembles for Monitoring Biomembrane Transport in Real Time. *Angew. Chem. Int. Ed.* **2014,** *53*, 2762-2765.
(11) Norouzy, A.; Azizi, Z.; Nau Werner, M. Indicator Displacement Assays Inside Live Cells. *Angew. Chem. Int. Ed.* **2014,** *54*, 792-795.
(12) Peng, S.; Pan, Y.-C.; Wang, Y.; Xu, Z.; Chen, C.; Ding, D.; Wang, Y.; Guo, D.-S. Sequentially Programmable and Cellularly Selective Assembly of Fluorescent Polymerized Vesicles for Monitoring Cell Apoptosis. *Adv. Sci.* **2017,** *4*, 1700310.
(13) Wang, K.; Guo, D.-S.; Zhao, M.-Y.; Liu, Y. A Supramolecular Vesicle Based on the Complexation of p-Sulfonatocalixarene with Protamine and its Trypsin-Triggered Controllable-Release Properties. *Chem. Eur. J.* **2016,** *22*, 1475-1483.
(14) Bockus, A. T.; Smith, L. C.; Grice, A. G.; Ali, O. A.; Young, C. C.; Mobley, W.; Leek, A.; Roberts, J. L.; Vinciguerra, B.; Isaacs, L.; Urbach, A. R. Cucurbit[7]uril–Tetramethylrhodamine Conjugate for Direct Sensing and Cellular Imaging. *J. Am. Chem. Soc.* **2016,** *138*, 16549-16552.
(15) Beatty, M. A.; Borges-González, J.; Sinclair, N. J.; Pye, A. T.; Hof, F. Analyte-Driven Disassembly and Turn-On Fluorescent Sensing in Competitive Biological Media. *J. Am. Chem. Soc.* **2018,** *140*, 3500-3504.
(16) Liu, Y.; Perez, L.; Mettry, M.; Easley, C. J.; Hooley, R. J.; Zhong, W. Self-Aggregating Deep Cavitand Acts as a Fluorescence Displacement Sensor for Lysine Methylation. *J. Am. Chem. Soc.* **2016,** *138*, 10746-9.
(17) Dsouza, R. N.; Hennig, A.; Nau, W. M. Supramolecular tandem enzyme assays. *Chem.* **2012,** *18*, 3444-59.
(18) Liu, Y.; Lee, J.; Perez, L.; Gill, A. D.; Hooley, R. J.; Zhong, W. Selective Sensing of Phosphorylated Peptides and Monitoring Kinase and Phosphatase Activity with a Supramolecular Tandem Assay. *J. Am. Chem. Soc.* **2018,** *140*, 13869-13877.
(19) Biedermann, F.; Hathazi, D.; Nau, W. M. Associative chemosensing by fluorescent macrocycle-dye complexes - a versatile enzyme assay platform beyond indicator displacement. *Chem. Commun.* **2015,** *51*, 4977-80.
(20) Florea, M.; Kudithipudi, S.; Rei, A.; Gonzalez-Alvarez, M. J.; Jeltsch, A.; Nau, W. M. A fluorescence-based supramolecular tandem assay for monitoring lysine methyltransferase activity in homogeneous solution. *Chem.* **2012,** *18*, 3521-8.

(21) Ghale, G.; Kuhnert, N.; Nau, W. M. Monitoring Stepwise Proteolytic Degradation of Peptides by Supramolecular Domino Tandem Assays and Mass Spectrometry for Trypsin and Leucine Aminopeptidase. *Nat. Prod. Commun.* **2012,** *7*, 1934578X1200700315.
(22) Stahl, A.; Lazar, A. I.; Muchemu, V. N.; Nau, W. M.; Ullrich, M. S.; Hennig, A. A fluorescent, supramolecular chemosensor to follow steroid depletion in bacterial cultures. *Anal. Bioanal.Chem.* **2017,** *409*, 6485-6494.
(23) Minami, T.; Esipenko, N. A.; Akdeniz, A.; Zhang, B.; Isaacs, L.; Anzenbacher, P. Multianalyte Sensing of Addictive Over-the-Counter (OTC) Drugs. *J. Am. Chem. Soc.* **2013,** *135*, 15238-15243.
(24) Shcherbakova, E. G.; Zhang, B.; Gozem, S.; Minami, T.; Zavalij, P. Y.; Pushina, M.; Isaacs, L. D.; Anzenbacher Jr, P. Supramolecular Sensors for Opiates and Their Metabolites. *J. Am. Chem. Soc.* **2017,** *139*, 14954-14960.
(25) Shah, K.; Hassan, E.; Ahmed, F.; Anis, I.; Rabnawaz, M.; Shah, M. R. Novel fluorene-based supramolecular sensor for selective detection of amoxicillin in water and blood. *Ecotoxicol. Environ. Saf.* **2017,** *141*, 25-29.
(26) Sinn, S.; Spuling, E.; Bräse, S.; Biedermann, F. Rational design and implementation of a cucurbit[8]uril-based indicator-displacement assay for application in blood serum. *Chem. Sci.* **2019**.
(27) Garnett, G. A.; Daze, K. D.; Pena Diaz, J. A.; Fagen, N.; Shaurya, A.; Ma, M. C.; Collins, M. S.; Johnson, D. W.; Zakharov, L. N.; Hof, F. Attraction by repulsion: compounds with like charges undergo self-assembly in water that improves in high salt and persists in real biological fluids. *Chem. Commun.* **2016,** *52*, 2768-71.
(28) Potyrailo, R. A.; Mirsky, V. M. Combinatorial and High-Throughput Development of Sensing Materials: The First 10 Years. *Chem. Rev.* **2008,** *108*, 770-813.
(29) Potyrailo, R.; Rajan, K.; Stoewe, K.; Takeuchi, I.; Chisholm, B.; Lam, H. Combinatorial and High-Throughput Screening of Materials Libraries: Review of State of the Art. *ACS Comb. Sci.* **2011,** *13*, 579-633.
(30) Briehn, C. A.; Schiedel, M.-S.; Bonsen, E. M.; Schuhmann, W.; Bäuerle, P. Single-Compound Libraries of Organic Materials: From the Combinatorial Synthesis of Conjugated Oligomers to Structure–Property Relationships. *Angew. Chem. Int. Ed.* **2001,** *40*, 4680-4683.

(31) Lee, J.-S.; Kim, H. K.; Feng, S.; Vendrell, M.; Chang, Y.-T. Accelerating fluorescent sensor discovery: unbiased screening of a diversity-oriented BODIPY library. *Chem. Commun.* **2011,** *47*, 2339-2341.
(32) Zhai, D.; Lee, S.-C.; Vendrell, M.; Leong, L. P.; Chang, Y.-T. Synthesis of a Novel BODIPY Library and Its Application in the Discovery of a Fructose Sensor. *ACS Comb. Sci.* **2012,** *14*, 81-84.
(33) Schiedel, M.-S.; Briehn, C. A.; Bäuerle, P. Single-Compound Libraries of Organic Materials: Parallel Synthesis and Screening of Fluorescent Dyes. *Angew. Chem. Int. Ed.* **2001,** *40*, 4677-4680.
(34) Vendrell, M.; Zhai, D.; Er, J. C.; Chang, Y.-T. Combinatorial Strategies in Fluorescent Probe Development. *Chem. Rev.* **2012,** *112*, 4391-4420.
(35) Rosania, G. R.; Lee, J. W.; Ding, L.; Yoon, H.-S.; Chang, Y.-T. Combinatorial Approach to Organelle-Targeted Fluorescent Library Based on the Styryl Scaffold. *J. Am. Chem. Soc.* **2003,** *125*, 1130-1131.
(36) Beatty, M. A.; Busmann, J. A.; Fagen, N. G.; Garnett, G. A. E.; Hof, F. A clip-like host that undergoes self-assembly and competitive guest-induced disassembly in water. *Supramol. Chem.* **2018**, 1-7.
(37) Beatty, M. A.; Pye, A. T.; Shaurya, A.; Kim, B.; Selinger, A. J.; Hof, F. Using reversible non-covalent and covalent bonds to create assemblies and equilibrating molecular networks that survive 5 molar urea. *Org. Biomol. Chem.* **2019,** *17*, 2081-2086.
(38) Umali, A. P.; LeBoeuf, S. E.; Newberry, R. W.; Kim, S.; Tran, L.; Rome, W. A.; Tian, T.; Taing, D.; Hong, J.; Kwan, M.; Heymann, H.; Anslyn, E. V. Discrimination of flavonoids and red wine varietals by arrays of differential peptidic sensors. *Chem. Sci.* **2011,** *2*, 439-445.
(39) Gade, A. M.; Meadows, M. K.; Ellington, A. D.; Anslyn, E. V. Differential array sensing for cancer cell classification and novelty detection. *Org. Biomol. Chem.* **2017,** *15*, 9866-9874.
(40) Peacor, B. C.; Ramsay, C. M.; Waters, M. L. Fluorogenic sensor platform for the histone code using receptors from dynamic combinatorial libraries. *Chem. Sci.* **2017,** *8*, 1422-1428.
(41) Minaker, S. A.; Daze, K. D.; Ma, M. C. F.; Hof, F. Antibody-Free Reading of the Histone Code Using a Simple Chemical Sensor Array. *J. Am. Chem. Soc.* **2012,** *134*, 11674-11680.

(42) Palacios, M. A.; Nishiyabu, R.; Marquez, M.; Anzenbacher, P. Supramolecular Chemistry Approach to the Design of a High-Resolution Sensor Array for Multianion Detection in Water. *J. Am. Chem. Soc.* **2007,** *129*, 7538-7544.
(43) Pode, Z.; Peri-Naor, R.; Georgeson, J. M.; Ilani, T.; Kiss, V.; Unger, T.; Markus, B.; Barr, H. M.; Motiei, L.; Margulies, D. Protein recognition by a pattern-generating fluorescent molecular probe. *Nat. Nanotechnol.* **2017,** *12*, 1161.
(44) Lapachinske, S. F.; Okai, G. G.; dos Santos, A.; de Bairros, A. V.; Yonamine, M. Analysis of cocaine and its adulterants in drugs for international trafficking seized by the Brazilian Federal Police. *Forensic Sci. Int.* **2015,** *247*, 48-53.
(45) Stewart, S.; Ivy, M. A.; Anslyn, E. V. The use of principal component analysis and discriminant analysis in differential sensing routines. *Chem. Soc. Rev.* **2014,** *43*, 70-84.
(46) Aps, J. K. M.; Martens, L. C. Review: The physiology of saliva and transfer of drugs into saliva. *Forensic Sci. Int.* **2005,** *150*, 119-131.
(47) Sonzini, S.; McCune, J. A.; Ravn, P.; Scherman, O. A.; van der Walle, C. F. A simple supramolecular assay for drug detection in urine. *Chem. Commun.* **2017,** *53*, 8842-8845.
(48) Navarro, M.; Pichini, S.; Farré, M.; Ortuño, J.; Roset, P. N.; Segura, J.; de la Torre, R. Usefulness of Saliva for Measurement of 3,4-Methylenedioxymethamphetamine and Its Metabolites: Correlation with Plasma Drug Concentrations and Effect of Salivary pH. *Clin. Chem.* **2001,** *47*, 1788-1795.
(49) Ellefsen, K. N.; Concheiro, M.; Pirard, S.; Gorelick, D. A.; Huestis, M. A. Oral fluid cocaine and benzoylecgonine concentrations following controlled intravenous cocaine administration. *Forensic Sci. Int.* **2016,** *260*, 95-101.
(50) Jenkins, A. J.; Oyler, J. M.; Cone, E. J. Comparison of Heroin and Cocaine Concentrations in Saliva with Concentrations in Blood and Plasma. *J. Anal. Toxicol.* **1995,** *19*, 359-374.
(51) Feyerabend, C.; Higenbottam, T.; Russell, M. A. Nicotine concentrations in urine and saliva of smokers and non-smokers. *Br. Med. J.* **1982,** *284*, 1002-1004.
(52) Cone, E. J.; Oyler, J.; Darwin, W. D. Cocaine Disposition in Saliva Following Intravenous, Intranasal, and Smoked Administration. *J. Anal. Toxicol.* **1997,** *21*, 465-475.

For Table of Contents Only

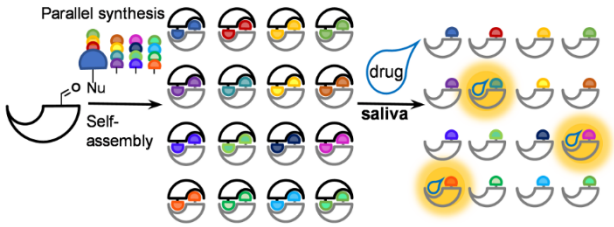

Supporting information
For

Parallel Synthesis and Screening of Supramolecular Chemosensors to Identify Fluorescent Turn-On Sensors of Drugs in Saliva

Meagan A. Beatty, Allison J. Selinger, YuQi Li, Fraser Hof

1. General methods and materials

^{1}H, ^{13}C, and 1D DOSY were recorded on a Bruker Avance Neo 500 MHz spectrometer unless otherwise indicated and processed with MestReNova by Mestrelab Research S.L. Deuterated solvents were purchased from Sigma Aldrich and NaH_2PO_4/Na_2HPO_4 (50 mM, pD 7.4) in D_2O were prepared, and the pD was adjusted with 1 M NaOD/DCl solutions. Accurate mass spectra determinations for novel compounds were done on a Thermo Scientific Ultimate 3000 ESI-Orbitrap Exactive. Purities were determined using a Waters UPLC-MS equipped with UV/Vis and QDa detector, with an Aquity UPLC BEH C18 1.7 uM (21 x 50 mm) column run with a gradient of 80% H_2O (+0.4% FA)/20% CH_3CN (+0.4% FA) to 50% H_2O (+0.4% FA)/50% CH_3CN (+0.4% FA) over 4 minutes at 0.6ml/min. All UV-Vis and fluorescence titrations and spectra were collected on a BioTek Cytation-5. Titrations and dilutions were conducted in NUNC black-walled, optical bottom 96-well plates. Infrared (IR) spectra were obtained using a Perkin Elmer 1000 FT-IR spectrometer. Data are represented as follows: frequency of absorption (cm^{-1}), intensity of absorption (s = strong, m = medium, w = weak, br = broad). Melting points were collected on a Gallenkamp Melting Point apparatus.
Compound **1** was prepared following literature protocol.[1] Heterocyclic compounds were synthesized from previously reported literature.[2-4]
All drugs except nicotine were purchased through Sigma Aldrich in 1mg/ml ampules dissolved in methanol or acetonitrile. To avoid adding organic solvent to DD array, the ampules were evaporated of organic solvent over a gentle stream of nitrogen overnight. The residue was re-dissolved in water and aliquoted to form stock solutions (1 mM) in NaH_2PO_4/Na_2HPO_4 (10 mM, pH 7.4). *S*-(-)-nicotine was purchased from Alfa Aesar. Stock solutions of DimerDyes 1, 4, 8, 12, 13 (1 mM) were prepared in NaH_2PO_4/Na_2HPO_4 (10 mM, pH 7.4) with concentrations accurately checked against a reference standard by quantitative NMR before being further diluted to a working stock (200 μM).

a. 1D DOSY procedure

For each DOSY experiment, the 90° pulse is determined by measuring the pulse length at 360° by a zg pulse sequence and dividing by four. The T1 relaxation was estimated through an inversion recovery (t1ir1d) pulse sequence. The relaxation time for each experiment was set to be 10-times the estimated T1. For each experiment, the Δ was set to 50 or 100 ms. The δ was determined by finding a 90-95% intensity difference between the first and last spectra in the power array via a stebpgp1s1d pulse program, see calculations below for δ used for each experiment. The pulse sequences used for 1D DOSY was stebpgp1s. After pre-processing through TopSpin, the area under the peaks of interest was selected and plotted as a function of the field gradient strength (G). These points were fitted to extract the diffusion coefficient, D. The hydrodynamic radius, r_H, was calculated with Stokes-Einstein equation with the following parameters: viscosity of water 8.7 $x10^{-4}$ Pa·s at 300 K.

b. Fluorescence titrations in diluted saliva

Saliva was prepared for handling by centrifugation (3400 rpm, 15 min) at 4°C to remove suspended solids. The supernatant was pipetted into a second conical tube containing an equal volume of water to reduce viscosity and foaming. To avoid multiple, foam-inducing transfers of saliva to form stocks, each DimerDye was directly pipetted into empty wells of a NUNC black-walled plate in a set of triplicates. The 1:1 saliva:water mixture was added to form a final [DD] = 12 μM at 100 μL. Separately, each drug (nicotine, MDMA, cocaine) was diluted in the 1:1 saliva:water mixture with a final [DD] = 12 μM and [drug] = 240 μM. This was serial diluted to achieve a [drug] = 240 μM – 4 μM.

c. General Synthesis of select DimerDyes

The protocol used for parallel synthesis and screening is described below. For all re-synthesized DimerDyes, the synthesis was as follows: **1** (50 mg) and Het4/8/9/12/13 (1.1 eq.) were dissolved in methanol (2 mL) along with morpholine (40 eq.) and heated at reflux for 12 hours. Cold ether was added to induce precipitation and the suspension was transferred to a 50 mL conical tube. After centrifugation (3400 rpm, 5 min) a pellet was formed and the supernatant was decanted and discarded. The pellet was re-suspended in fresh cold ether and the centrifugation, decanting process was repeated two more times. The pellet was re-dissolved in the indicated eluent composition and filtered. A Shimadzu HPLC with a 280 nm and 370 nm

detector was used to purify the final product with a Phenomenex Luna C18, 250 mm x 22 mm, 5 μM preparative column.

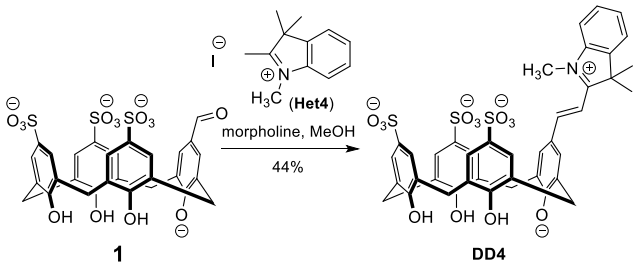

DD4. Het4 was prepared as previously reported.[2] Purified with a gradient of 85% H_2O (+0.1% TFA)/15% CH_3CN (+0.1% TFA) to 50% H_2O (+0.1% TFA)/50% CH_3CN (+0.1% TFA) over 20 minutes. The fractions were collected and lyophilized to yield a yellow/orange fluffy solid (27 mg, 44%). Mp: decomposed > 260°C. FT-IR (cm^{-1}): 3229 (br), 1585 (m), 1535 (w), 1479 (m), 1447 (w), 1292 (w), 1163 (s), 1135 (s), 1036 (s), 786 (m), 749 (w), 626 (s), 543 (m). ^1H NMR (500 MHz, D_2O): δ 7.79 (s, 1H), 7.78 (s, 1H), 7.63 (d, J = 16.3 Hz, 1H), 7.55 (s, 2H), 7.48 (s, 2H), 7.32 (s, 2H), 6.55 (d, J = 15.7 Hz, 1H), 6.35 (d, J = 6.7 Hz, 1H), 5.90 (br, 1H), 4.57 (d, J = 13.7 Hz , 2H), 4.27 (br, 1H), 4.10 (d, J = 12.2 Hz, 2H), 3.88 (br, 1H), 3.63 (d, J = 12.2 Hz, 2H), 3.54 (s, 3H), 3.43 (d, J = 13.7 Hz, 2H), 1.36 (s, 6H). ^{13}C NMR (76 MHz, DMSO): δ 180.7, 161.2, 153.9, 152.1, 151.4, 143.0, 141.9, 138.7, 138.5, 132.6, 129.7, 128.2, 127.9, 127.8, 127.2, 126.4, 126.2, 125.6, 122.6, 114.2, 108.4, 51.4, 33.7, 31.2, 30.6, 25.8. HR-MS (M^+ *m/z*): Calculated for $C_{41}H_{38}NO_{13}S_3^+$ 848.14998, Found 848.14938.

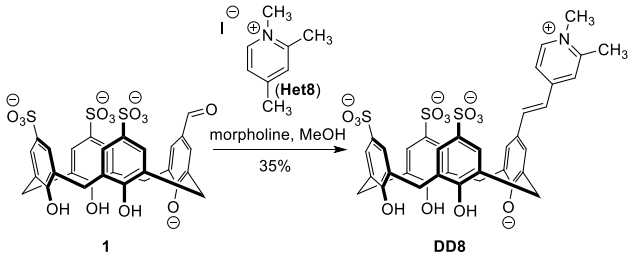

DD8. Het8 was prepared as previously reported.[3] Purified with a gradient of 90% H_2O (+0.1% TFA)/10% CH_3CN (+0.1% TFA) to 70% H_2O (+0.1% TFA)/30% CH_3CN (+0.1% TFA) over 23 minutes. The fractions were collected and lyophilized to yield a yellow fluffy solid (20 mg, 35%). Mp: decomposed > 300°C. FT-IR (cm^{-1}): 3288 (br), 1621 (m), 1598 (m), 1451 (w), 1132 (s), 1111 (s), 891 (w), 786 (w), 732 (w), 623 (s), 583 (s). ^1H NMR (500 MHz, D_2O): δ 7.69 (d, J = 1.4 Hz, 2H), 7.63 (d, J = 1.8 Hz, 2H), 7.36 (s, 2H), 7.14 (d, J = 6.1 Hz, 1H), 7.09 (s, 2H), 6.96 (s, 1H), 6.67 (d, J = 6.1 Hz, 1H), 6.67 (d, J = 15.5 Hz, 1H), 6.27 (d, J = 16.5 Hz, 1H), 4.34 (d, J = 3.5 Hz, 2H), 4.32 (d, J = 3.1 Hz, 2H), 3.53 (d, J = 13.4 Hz, 2H), 3.48 (d, J = 13.8 Hz, 2H), 0.79 (s, 3H), 0.54 (s, 3H). ^{13}C NMR (126 MHz, DMSO): δ 153.9, 152.3, 151.7, 149.6, 140.0, 139.7, 128.8, 127.4, 127.3, 127.2, 126.4, 126.3, 30.4, 18.2. HR-MS (M^+ *m/z*): Calculated for $C_{37}H_{34}NO_{13}S_3^+$ 796.11868, Found 796.11754.

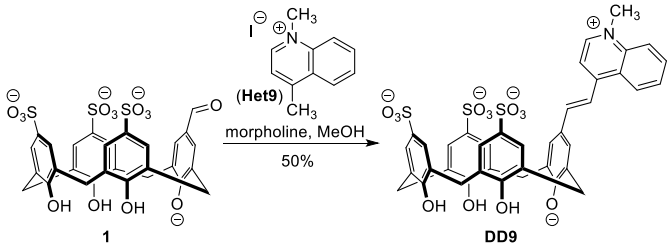

DD9. Het9 was prepared as previously reported.[3] Purified with a gradient of 85% H_2O (+0.1% TFA)/15% CH_3CN (+0.1% TFA) to 50% H_2O (+0.1% TFA)/50% CH_3CN (+0.1% TFA) over 18 minutes. The fractions were collected and lyophilized to yield an orange fluffy solid (30 mg, 50%). Mp: decomposed > 300°C. FT-IR (cm^{-1}): 3287 (br), 1593 (m), 1567 (m), 1535 (w), 1476 (w), 1449 (w), 1134 (s), 1109 (s), 1035 (s), 626 (s), 544 (s). ^1H NMR (500 MHz, D_2O): δ 7.81 (d, J = 2.3 Hz, 2H), 7.76 (d, J = 1.9 Hz, 2H), 7.67 (d, J = 8.6 Hz, 1H), 7.33 (s, 2H), 7.30 (d, J = 6.5 Hz, 1H), 7.17 (d, J = 6.5 Hz, 1H), 6.97 (s, 2H), 6.68 (br. 1H), 6.64 (d, J = 15.6 Hz, 1H), 6.47 (d, J = 16.2 Hz, 1H), 6.41 (br. 1H), 5.79 (d, J = 9.1 Hz, 1H), 4.45 (d, J = 13.6 Hz, 2H),

4.31 (d, J = 13.7 Hz, 2H), 3.60 (d, J = 13.1 Hz, 2H), 3.53 (d, J = 13.1 Hz, 2H), 2.05 (s, 3H). ^{13}C NMR (126 MHz, DMSO) δ: 153.0, 152.2, 150.5, 140.4, 138.2, 128.8, 128.1, 127.9, 127.7, 127.4, 126.9, 126.7, 125.6, 116.1, 43.6, 31.2, 30.9. HR-MS (M^+ *m/z*): Calculated for $C_{40}H_{34}NO_{13}S_3^+$ 832.11868, Found 832.11788.

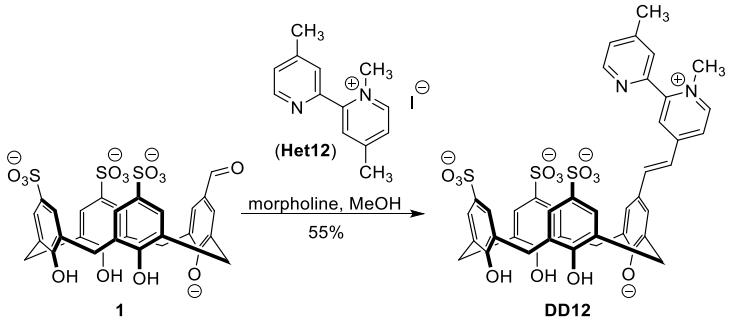

DD12. Het12 was prepared as previously reported.[3] Purified with a gradient of 85% H_2O (+0.01% TFA)/15% CH_3CN (+0.01% TFA) to 50% H_2O (+0.01% TFA)/50% CH_3CN (+0.01% TFA) over 23 minutes. The fractions were collected and lyophilized to yield an orange fluffy solid (35 mg, 55%). Mp: decomposed > 300°C. FT-IR (cm^{-1}): 3240 (br), 1615 (m), 1591 (m), 1453 (w), 1156 (s), 1111 (s), 1037 (s), 886 (w), 785 (w), 657 (m), 624 (s), 547 (s).). ^{1}H NMR (500 MHz, D_2O): δ 7.67 (d, J = 5.1 Hz, 1H), 7.69 (d, J = 2.1 Hz, 2H), 7.58 (br, 1H), 7.55 (d, J = 2.1 Hz, 2H), 7.42 (d, J = 6.1 Hz, 1H), 7.38 (s, 2H), 7.30 (s, 2H), 7.24 (s, 2H), 7.05 (d, J = 16.1 Hz, 1H), 6.80 (d, J = 16.1 Hz, 1H), 6.42 (s, 1H), 5.94 (br, 1H), 4.36 (d, J = 14.4 Hz, 2H), 4.33 (d, J = 14.4 Hz, 2H), 3.55 (d, J = 12.4 Hz, 2H), 3.52 (d, J = 12.8 Hz, 2H), 3.12 (s, 3H), 0.45 (s, 3H). ^{13}C NMR (126 MHz, DMSO): δ 154.1, 151.5, 146.9, 142.1, 140.0, 123.0, 129.1, 127.9, 127.7, 127.5, 127.0, 126.9, 125.2, 120.6, 46.1, 31.4, 31.1, 21.1. HR-MS (M^+ *m/z*): Calculated for $C_{42}H_{37}N_2O_{13}S_3^+$ 873.14523, Found 873.14435.

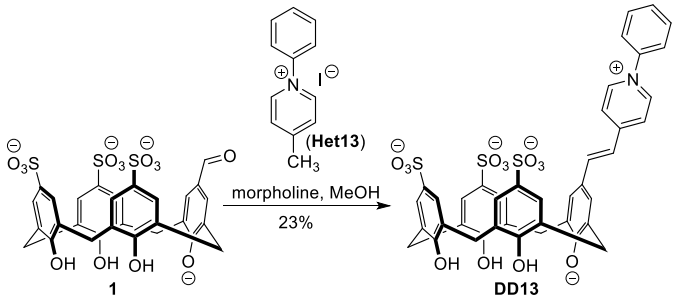

DD13. Het13 was prepared as previously reported.[4] Purified with a gradient of 85% H_2O (+0.1% TFA)/15% CH_3CN (+0.1% TFA) to 50% H_2O (+0.1% TFA)/50% CH_3CN (+0.1% TFA) over 20 minutes. The fractions were collected and lyophilized to yield an orange fluffy solid (14 mg, 23%). Mp decomposed > 280°C. FT-IR (cm^{-1}): 3229 (br), 1618 (m), 1587 (m), 1489 (w), 1451 (w), 1200 (s), 1133 (s), 1110 (s), 1036 (s), 878 (w), 760 (w), 624 (s), 549 (s). ^{1}H NMR (500 MHz, D_2O): δ 8.28 (d, J = 6.8 Hz, 2H), 7.72 (d, J = 7.0 Hz, 2H), 7.58 (s, 2H), 7.46 (d, J = 2.1 Hz, 2H), 7.40 (d, J = 2.1Hz, 2H), 7.30 (d, J = 15.8 Hz, 1H), 7.26 (s, 2H), 6.72 (d, J = 16.1 Hz, 1H), 6.18 (d, J = 6.92 Hz, 2H), 5.10 (br, 2H), 4.45 (d, J = 12.7 Hz, 2H), 4.27 (d, J = 12.7 Hz, 2H), 4.13 (br, 1H), 3.59 (d, J = 13.3 Hz, 2H), 3.45 (d, J = 12.7 Hz, 2H). ^{13}C NMR (126 MHz, DMSO): δ 155.0, 154.6, 151.5, 144.0, 143.3, 142.8, 139.9, 131.2, 130.6, 130.2, 129.3, 127.9, 127.8, 127.7, 127.5, 127.0, 126.9, 124.8, 123.7, 120.6, 31.5, 31.1. HR-MS (M^+ *m/z*): Calculated for $C_{41}H_{34}NO_{13}S_3^+$ 844.11868, Found 844.11786.

2. ^{1}H and ^{13}C NMR spectra

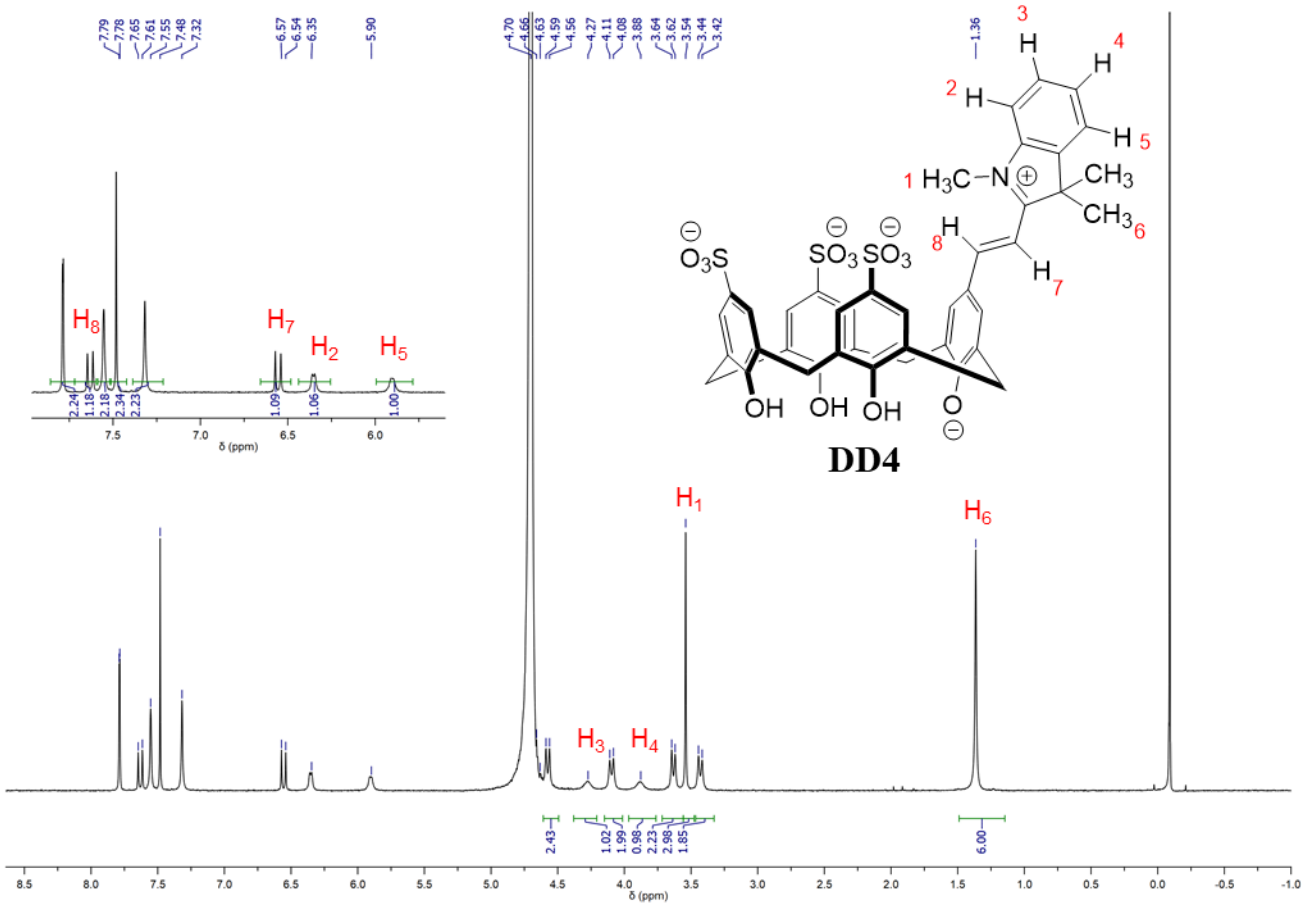

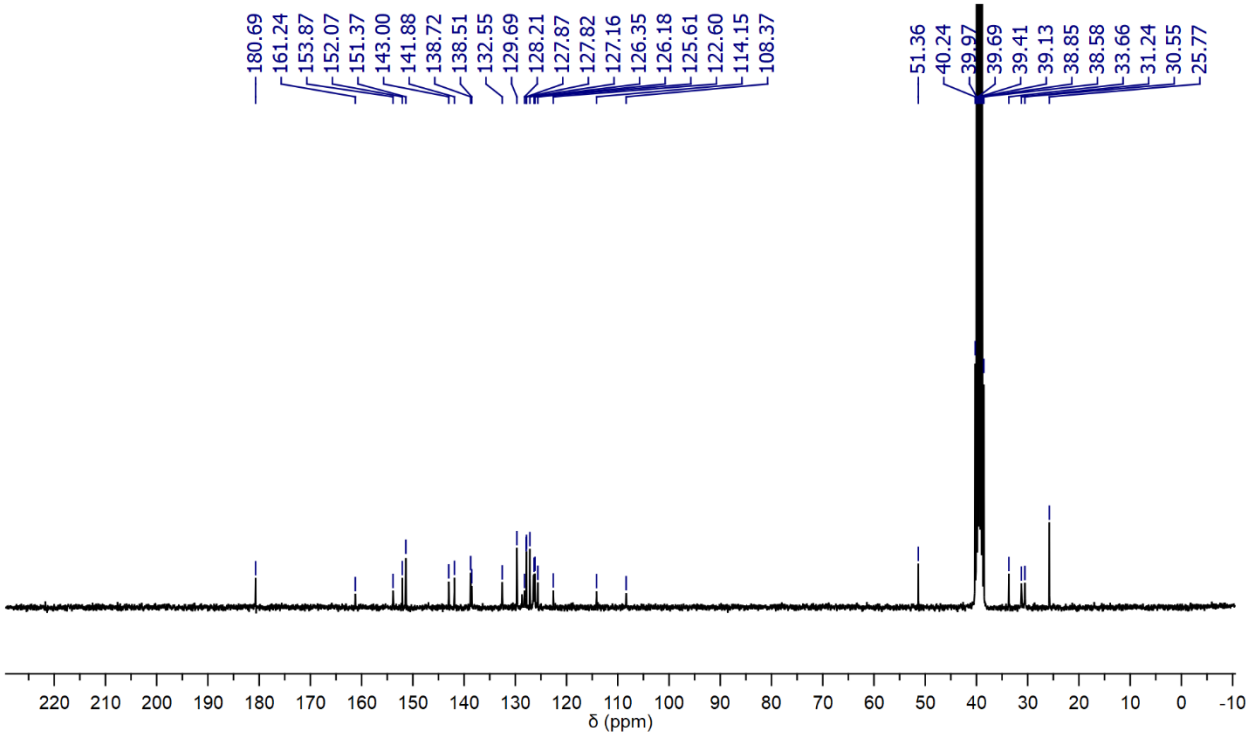

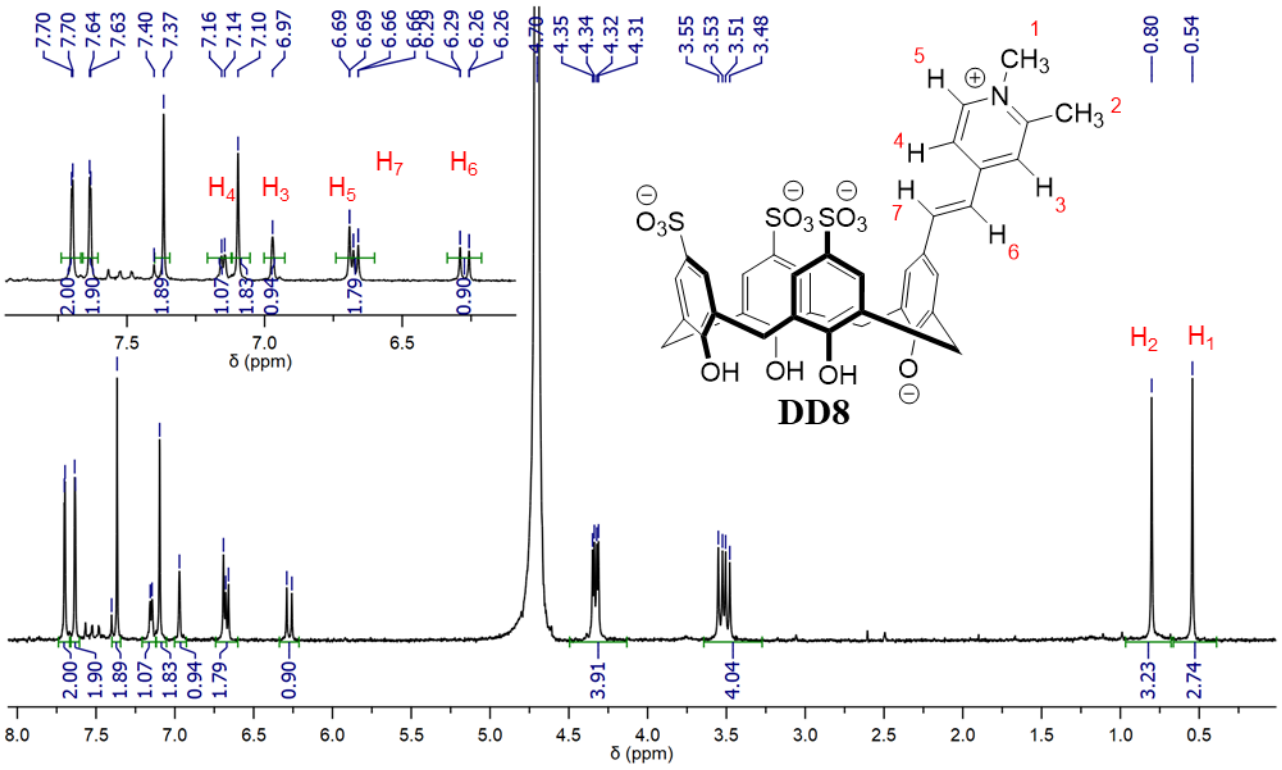
7.70
7.70
7.64
7.63
7.40
7.37
7.16
7.14
7.10
6.97
6.69
6.69
6.66
6.29
6.26
6.26
4.70
4.35
4.34
4.32
4.31
3.55
3.53
3.51
3.48
0.80
0.54
H4
H3
H5
H7
H6
2.00
1.90
1.89
1.07
1.83
0.94
1.79
0.90
7.5
7.0
6.5
δ (ppm)
O3S
SO3 SO3
OH OH OH
O
DD8
H2
H1
3.91
4.04
3.23
2.74
8.0
7.5
7.0
6.5
6.0
5.5
5.0
4.5
4.0
3.5
3.0
2.5
2.0
1.5
1.0
0.5
δ (ppm)

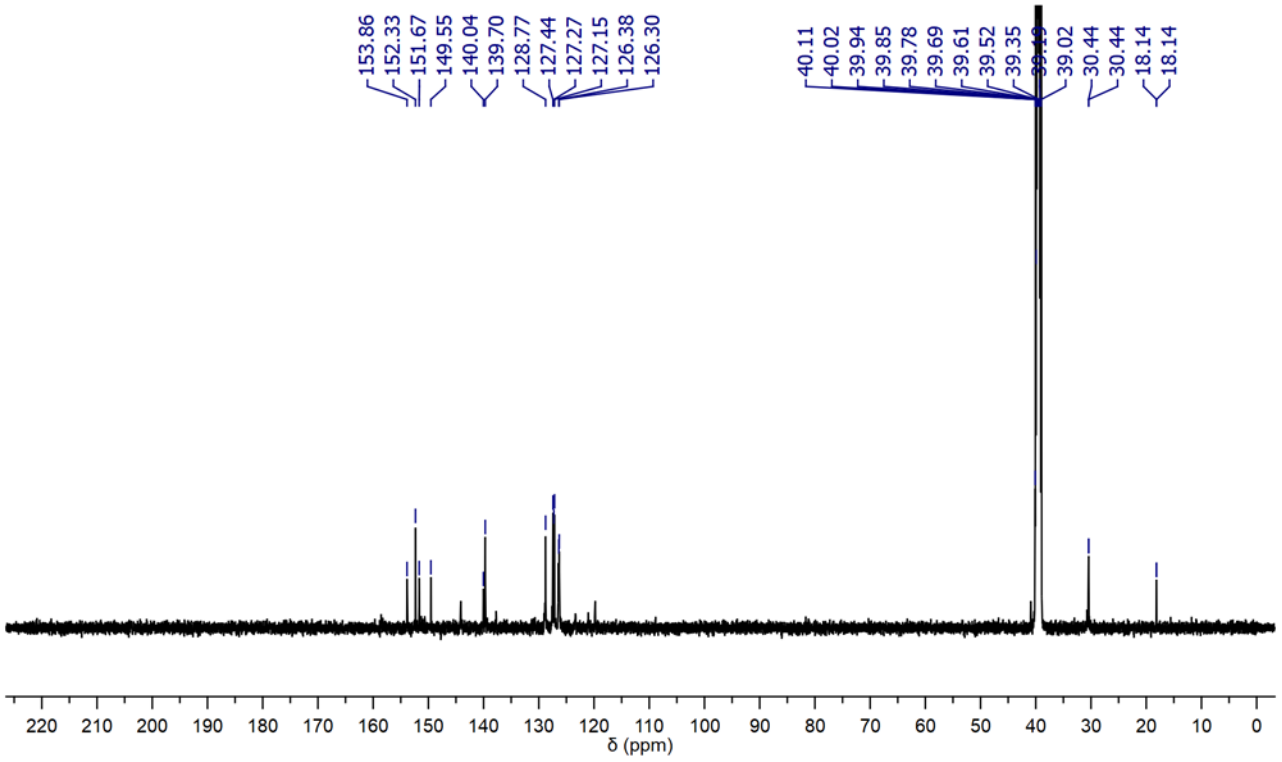
153.86
152.33
151.67
149.55
140.04
139.70
128.77
127.44
127.27
127.15
126.38
126.30
40.11
40.02
39.94
39.85
39.78
39.69
39.61
39.52
39.35
39.19
39.02
30.44
30.44
18.14
18.14
220
210
200
190
180
170
160
150
140
130
120
110
100
90
80
70
60
50
40
30
20
10
0
δ (ppm)

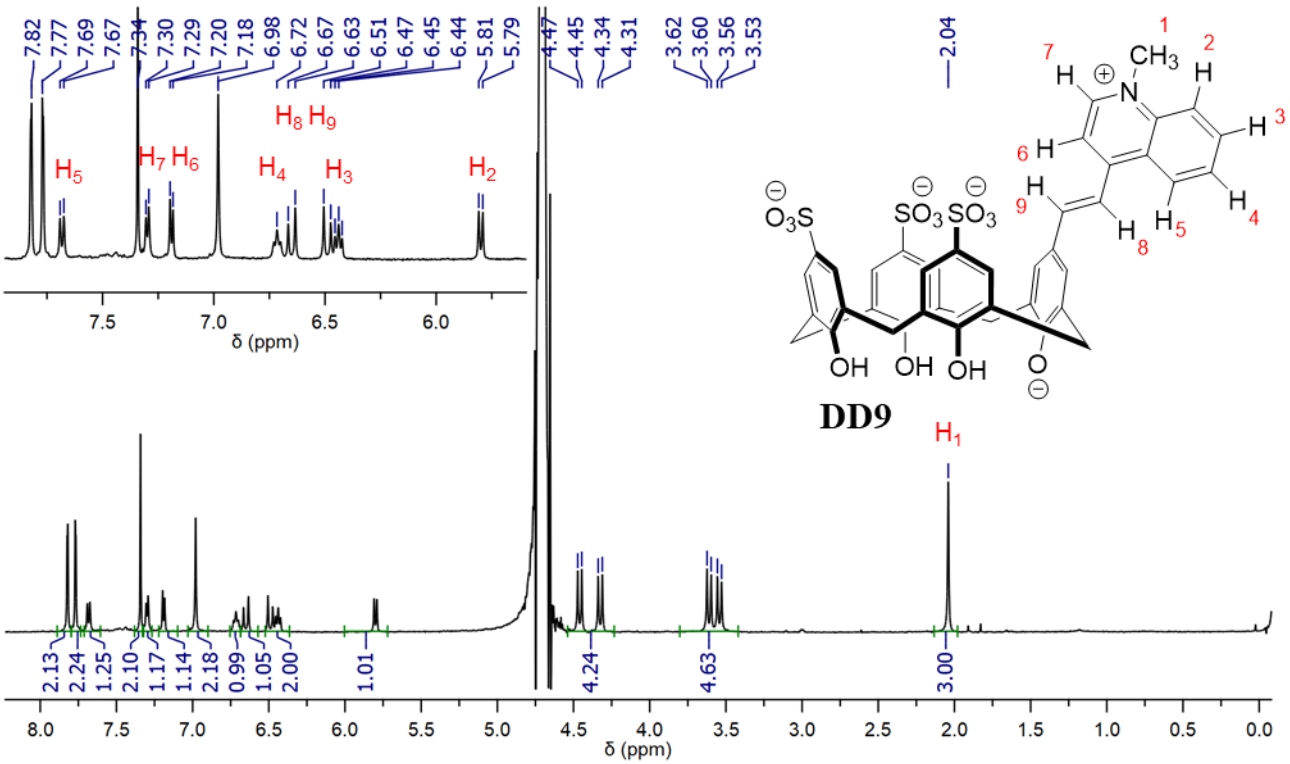
7.82
7.77
7.69
7.67
7.34
7.30
7.29
7.20
7.18
6.98
6.72
6.67
6.63
6.51
6.47
6.45
6.44
5.81
5.79
4.47
4.45
4.34
4.31
3.62
3.60
3.56
3.53
2.04
H5
H7 H6
H8 H9
H4
H3
H2
H1
δ (ppm)
2.13
2.24
1.25
2.10
1.17
1.14
2.18
0.99
1.05
2.00
1.01
4.24
4.63
3.00
DD9

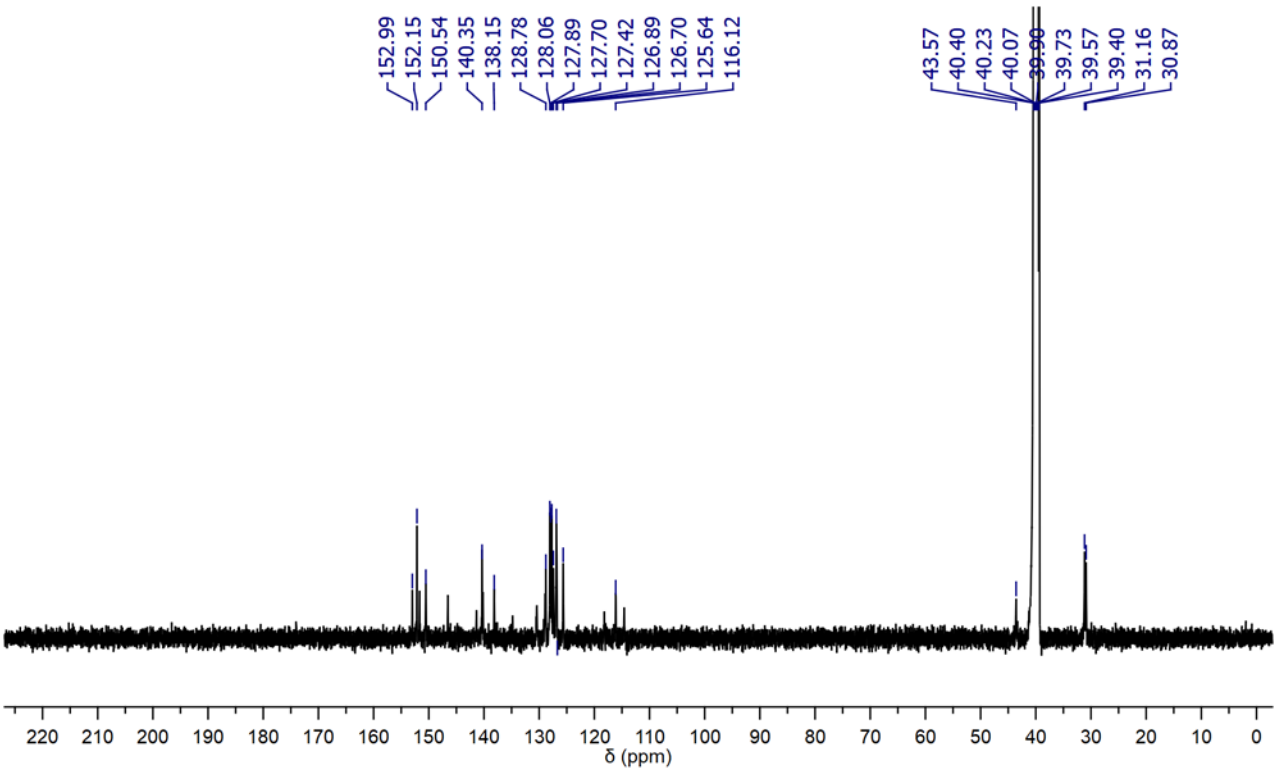
152.99
152.15
150.54
140.35
138.15
128.78
128.06
127.89
127.70
127.42
126.89
126.70
125.64
116.12
43.57
40.40
40.23
40.07
39.90
39.73
39.57
39.40
31.16
30.87
δ (ppm)

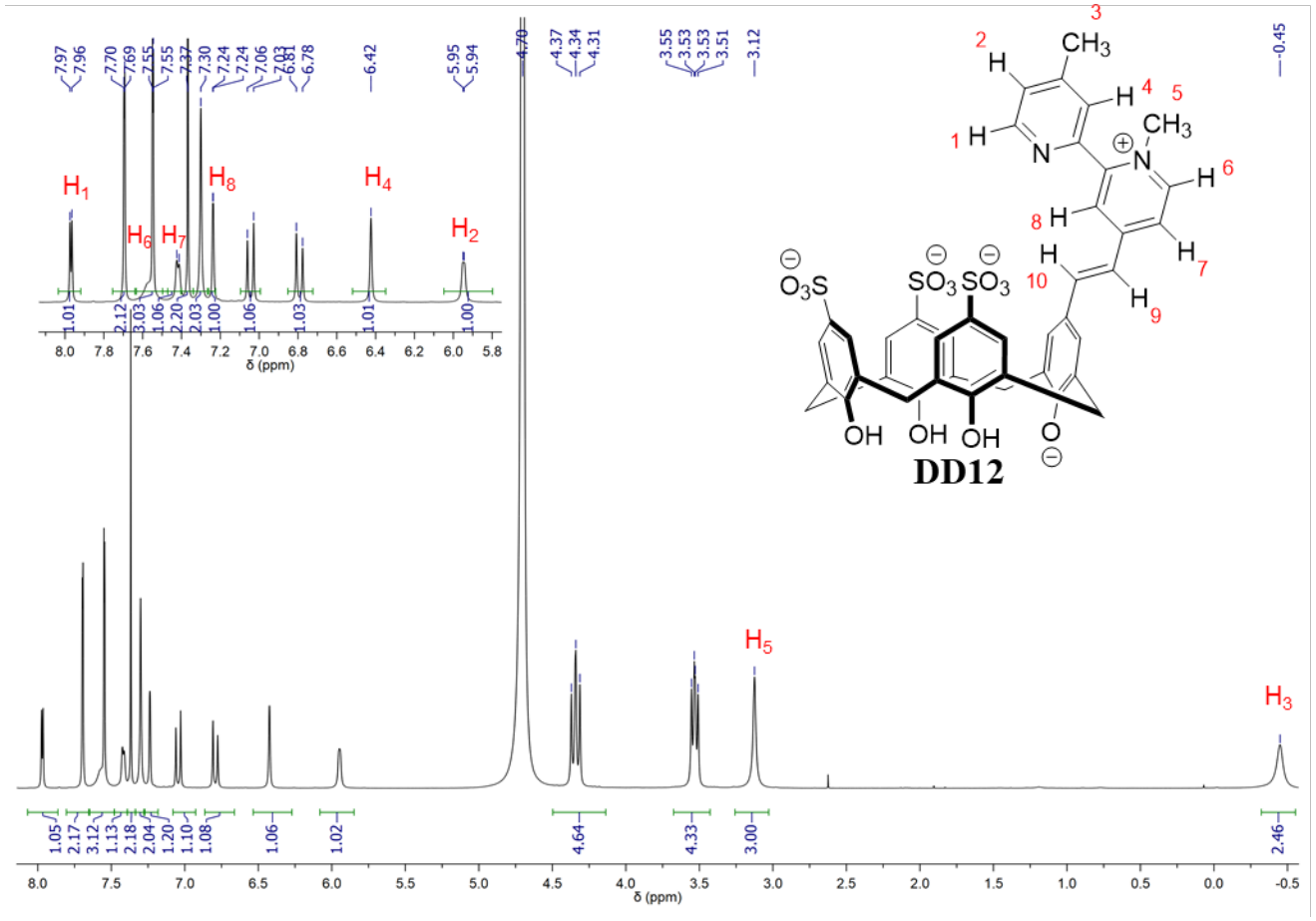
H1
H6
H7
H8
H4
H2
H5
H3
δ (ppm)
DD12

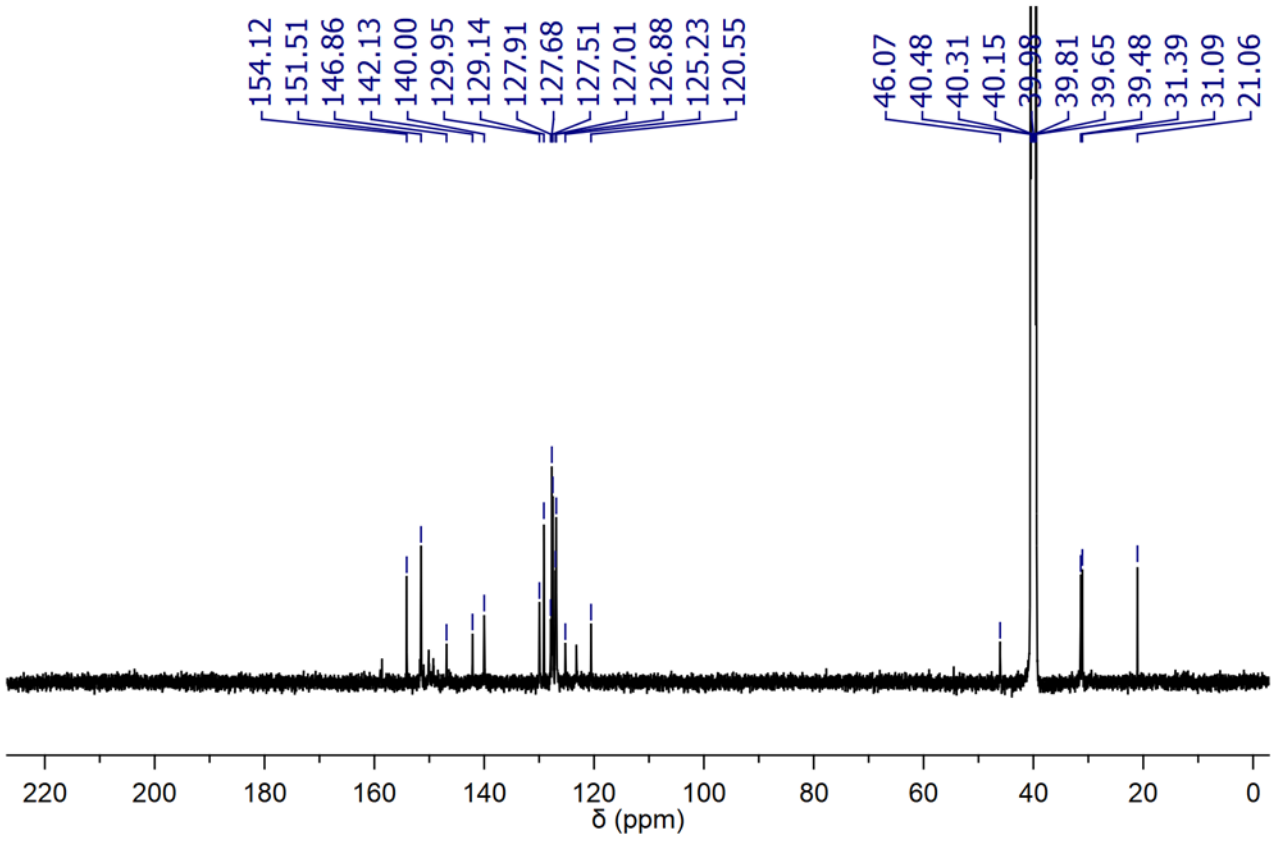
δ (ppm)

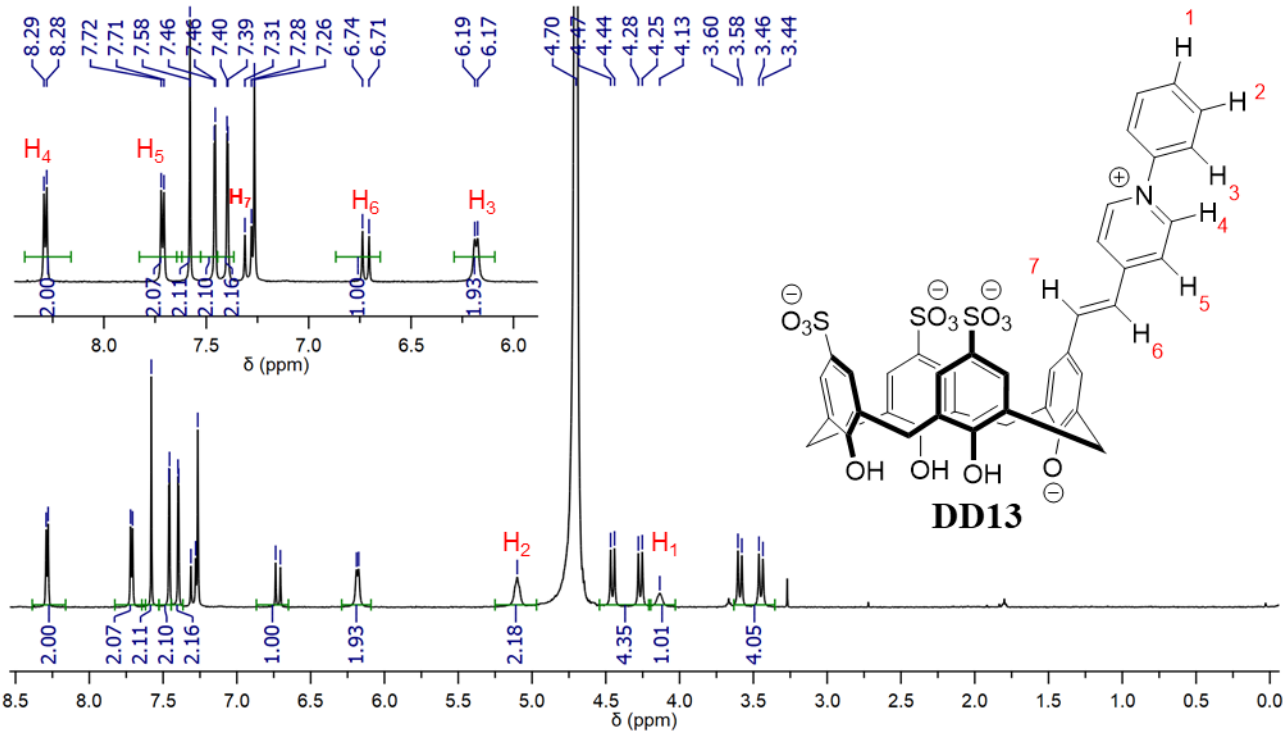
8.29
8.28
7.72
7.71
7.58
7.46
7.40
7.39
7.31
7.28
7.26
6.74
6.71
6.19
6.17
4.70
4.47
4.44
4.28
4.25
4.13
3.60
3.58
3.46
3.44
H4
H5
H7
H6
H3
H2
H1
2.00
2.07
2.11
2.10
2.16
1.00
1.93
2.18
4.35
1.01
4.05
δ (ppm)
DD13

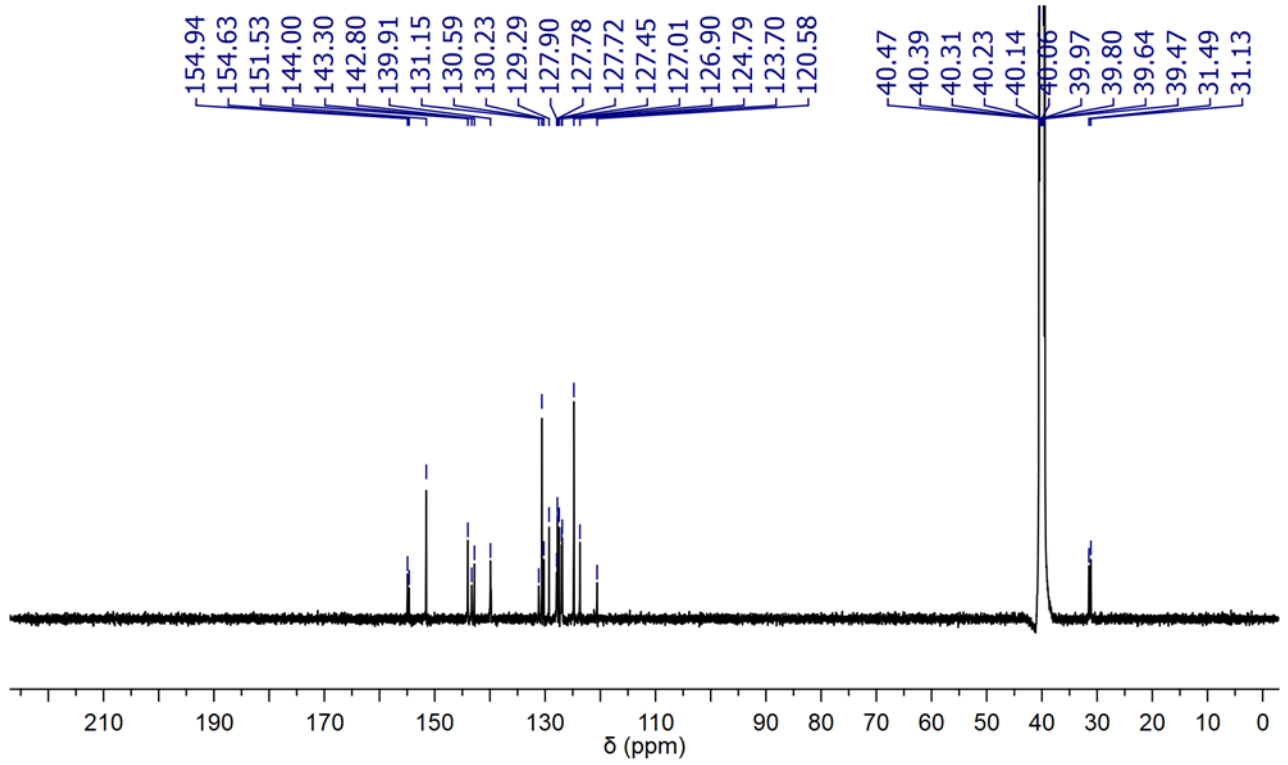
154.94
154.63
151.53
144.00
143.30
142.80
139.91
131.15
130.59
130.23
129.29
127.90
127.78
127.72
127.45
127.01
126.90
124.79
123.70
120.58
40.47
40.39
40.31
40.23
40.14
40.06
39.97
39.80
39.64
39.47
31.49
31.13
δ (ppm)

3. Additional ^{1}H NMR characterization of dimer assembly

Table S1. Chemical shift differences between key resonances of **DD** and their respective **Het**.

	Het1	**DD1**	Δδ		**Het8**	**DD8**	Δδ
N-CH_3	4.33	0.66	3.67	H1	4.14	0.54	3.60
ortho	8.59	7.35	1.24	H2	2.56	0.79	1.77
meta	7.87	6.42	1.45	H3	8.47	6.66	1.81
				H4	7.62	7.15	0.47
				H5	8.47	6.68	1.79

	Het4	**DD4**	Δδ		**Het12**	**DD12**	Δδ
H1	4.00	3.54	0.46	H1	8.59	7.94	0.65
H6	1.55	1.36	0.19	H2	7.55	5.90	1.65
H2	7.70	6.35	1.35	H3	2.50	0.45	2.05
H3	7.59	4.27	3.32	H4	7.63	6.40	1.23
H4	7.57	3.88	3.69	H5	4.12	3.12	1.00
H5	7.78	5.90	1.88	H6	8.69	7.68	1.01
				H7	7.91	7.41	0.5
				H8	7.93	7.25	0.68

	Het9	**DD9**	Δδ		**Het13**	**DD13**	Δδ
H1	4.54	2.04	2.50	H1	7.59	4.13	3.46
H2	8.41	5.80	2.61	H2	7.59	5.10	2.49
H3	8.17	6.45	1.72	H3	7.59	6.17	1.42
H4	7.96	6.72	1.24	H4	8.79	8.28	0.51
H5	8.29	7.68	0.61				
H6	7.84	7.19	0.65				
H7	8.97	7.30	1.67				

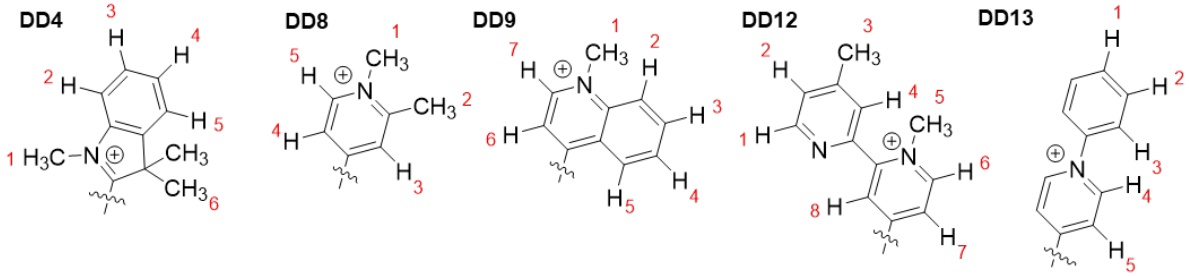

4. Development of parallel synthesis and screening method

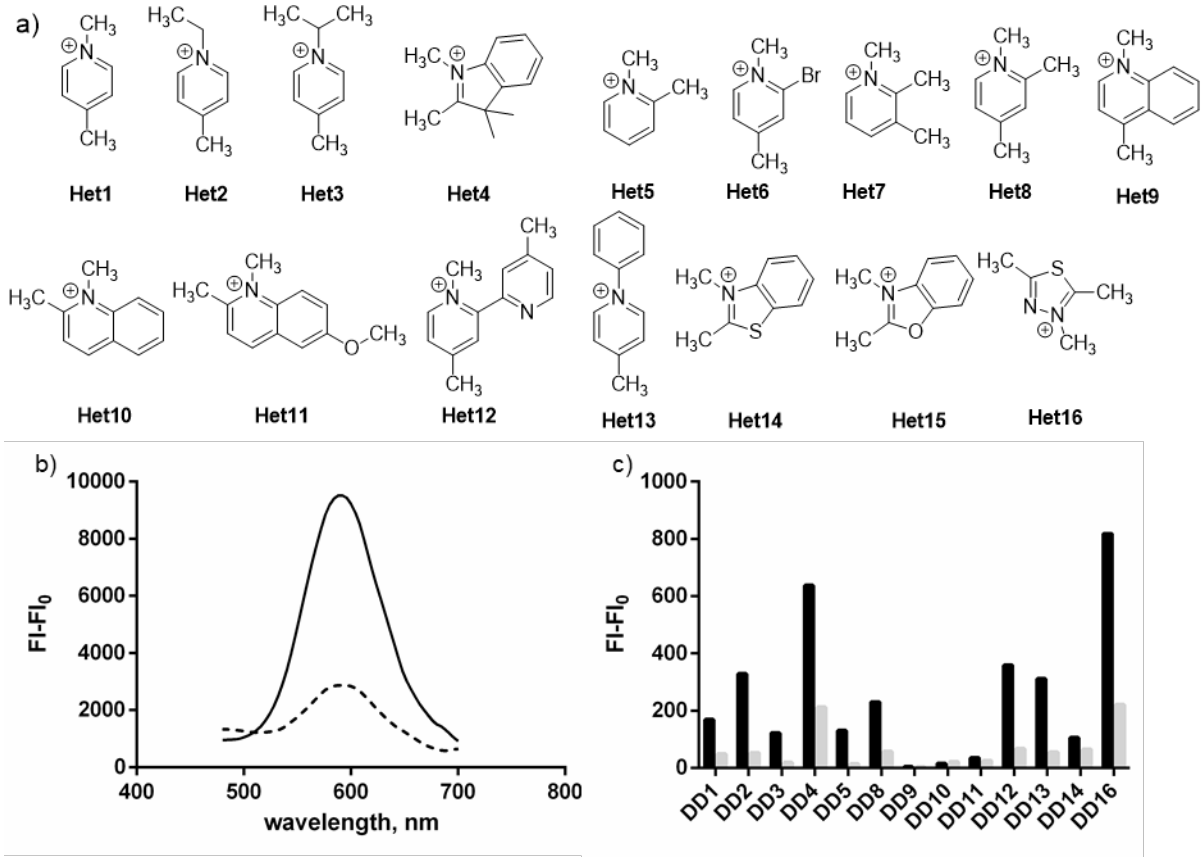

Figure S1. Establishing conditions that allow efficient synthesis of all DDs. a) **Het1-16** used for condensation reactions b) Fluorescence spectra ($\lambda_{ex.}$ 390 nm) of **DD1** with nicotine (50 μM) increases when changing the reaction time from 1.5 h (dotted line) to 6 h (solid line). c) The response of each crudely synthesized DD to nicotine (10 μM) after reacting with either 40 eq. of morpholine (black bars) or 20 eq. of morpholine (gray bars).

Procedure for parallel synthesis of DDs: An aluminum heating block (CombiBlocks, ChemGlass) held 4 dram vials which each contained a 1:1 mixture of **1** and one heterocyclic nucleophile (1.5 mM), along with morpholine (40 eq., 5 μL) in methanol (1 mL). The mixtures were capped, heated and stirred behind a blast shield for 6 hours at 50°C to afford coloured solutions. The solutions were sonicated to re-dissolve dried DimerDyes along the walls. The solutions were aliquoted (10 μL) into NUNC black-walled, clear-bottomed 96-well plates and dried in a 37°C oven for 4 hours. The dried pellets were re-suspended in phosphate buffer (10 mM, pH 7.4), centrifuged and mixed. Each solution was diluted by transferring aliquots into a separate 96-well plate containing the same phosphate buffer. Fluorescence endpoint measurements were taken for each DimerDye, the $\lambda_{ex.}$ and $\lambda_{em.}$ that were used are listed below. A stock of nicotine prepared in phosphate buffer was added to each well (10 μL for final concentration of 10 μM) and fluorescence endpoint measurements were collected again. The fluorescence differences between after and before nicotine were used to evaluate each DimerDye.

Table S2. Excitation and emission wavelengths used for crude DimerDye screening

	$\lambda_{ex.}$, nm	$\lambda_{em.}$, nm
DD1	380	575
DD2	390	575
DD3	390	575
DD4	480	560
DD5	390	575
DD8	380	575
DD9	440	680
DD10	450	600
DD11	440	630
DD12	410	615
DD13	420	620
DD14	470	565
DD16	420	555

5. UPLC-MS data of crude DimerDye reactions

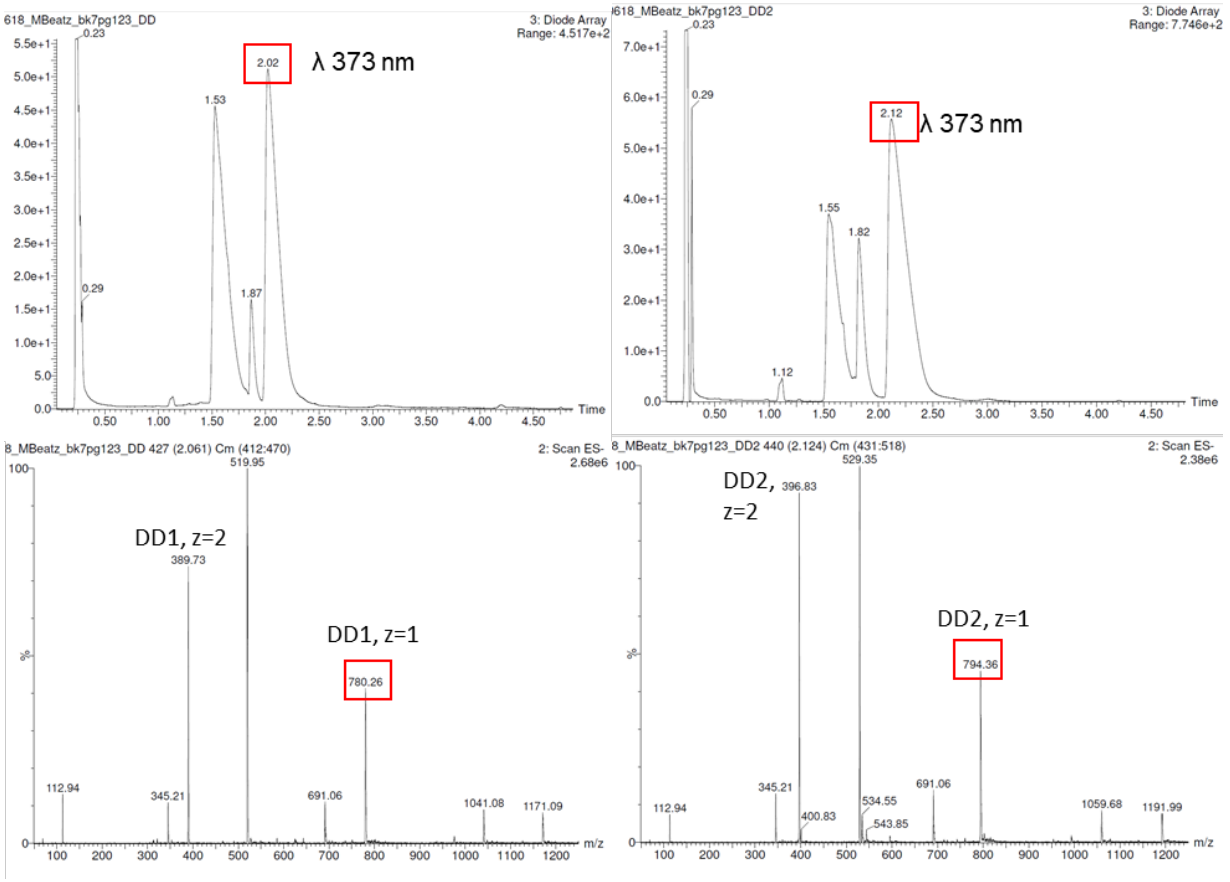

Figure S2. UPLC-MS traces confirm the partial synthesis of **DD1** (left) and **DD2** (right).

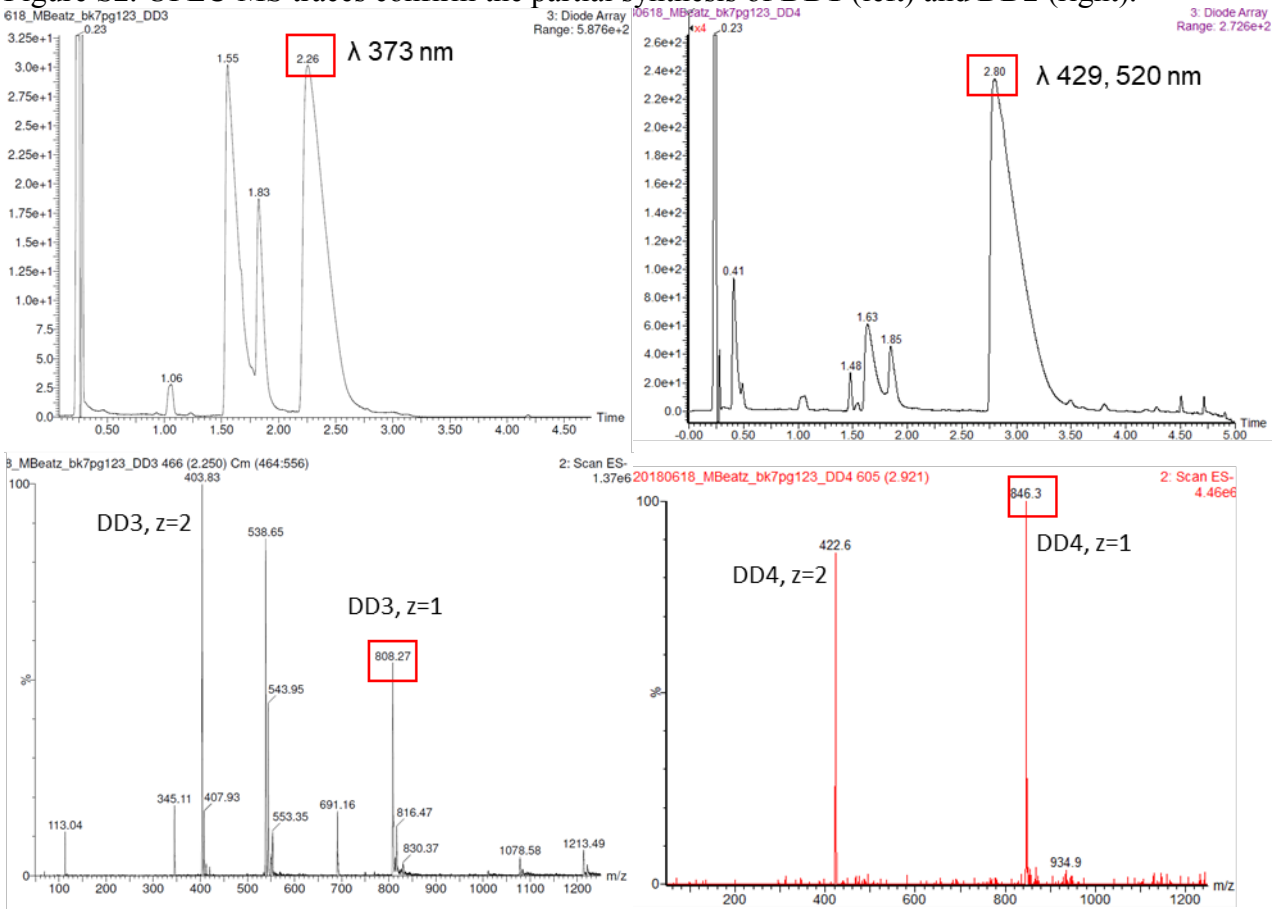

Figure S3. UPLC-MS traces confirm the partial synthesis of **DD3** (left) and **DD4** (right).

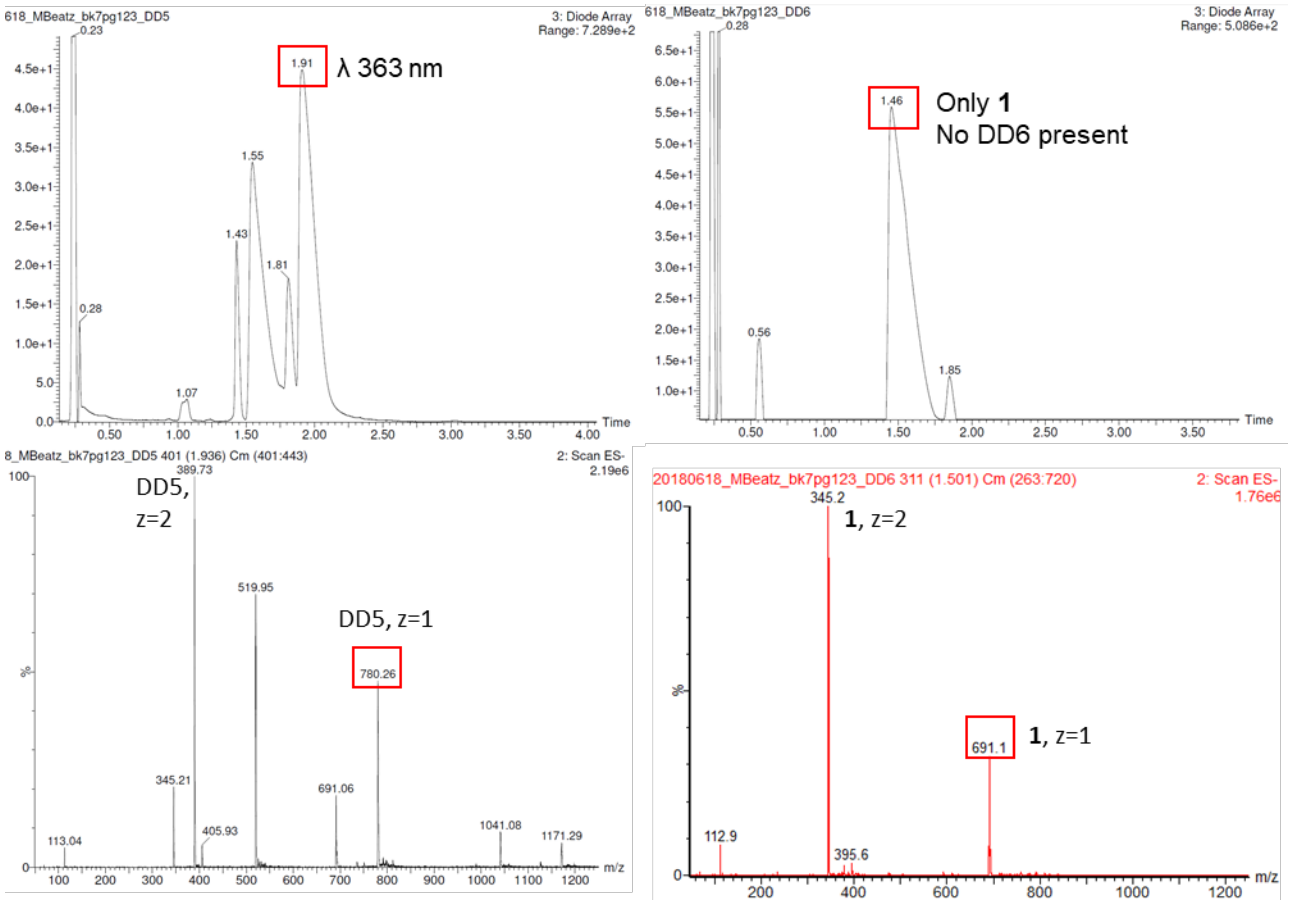

Figure S4. UPLC-MS traces confirm the partial synthesis of **DD5** (left) and a failed **DD6** (right) reaction.

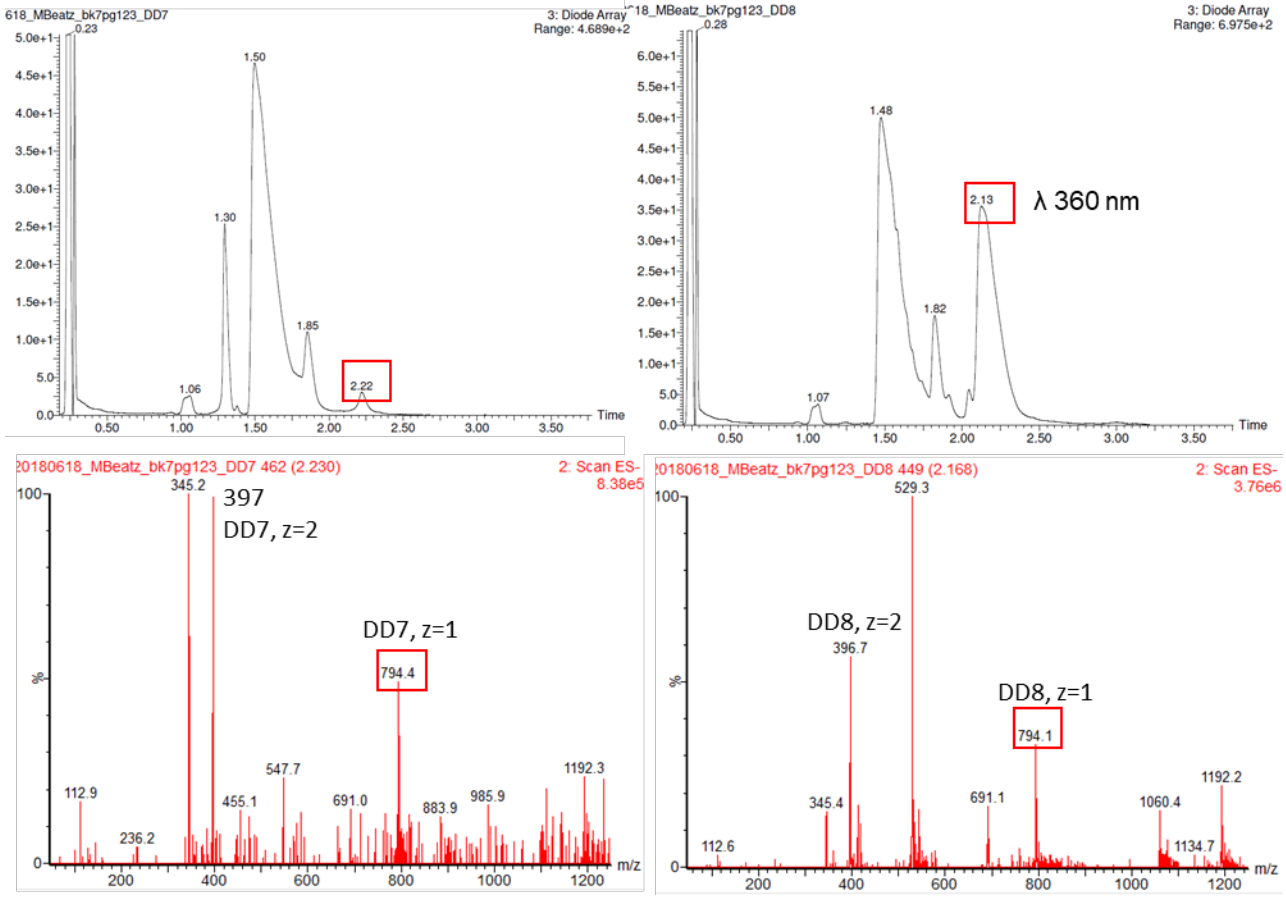

Figure S5. UPLC-MS traces show trace signs of **DD7** (left) and partial formation of **DD8** (right).

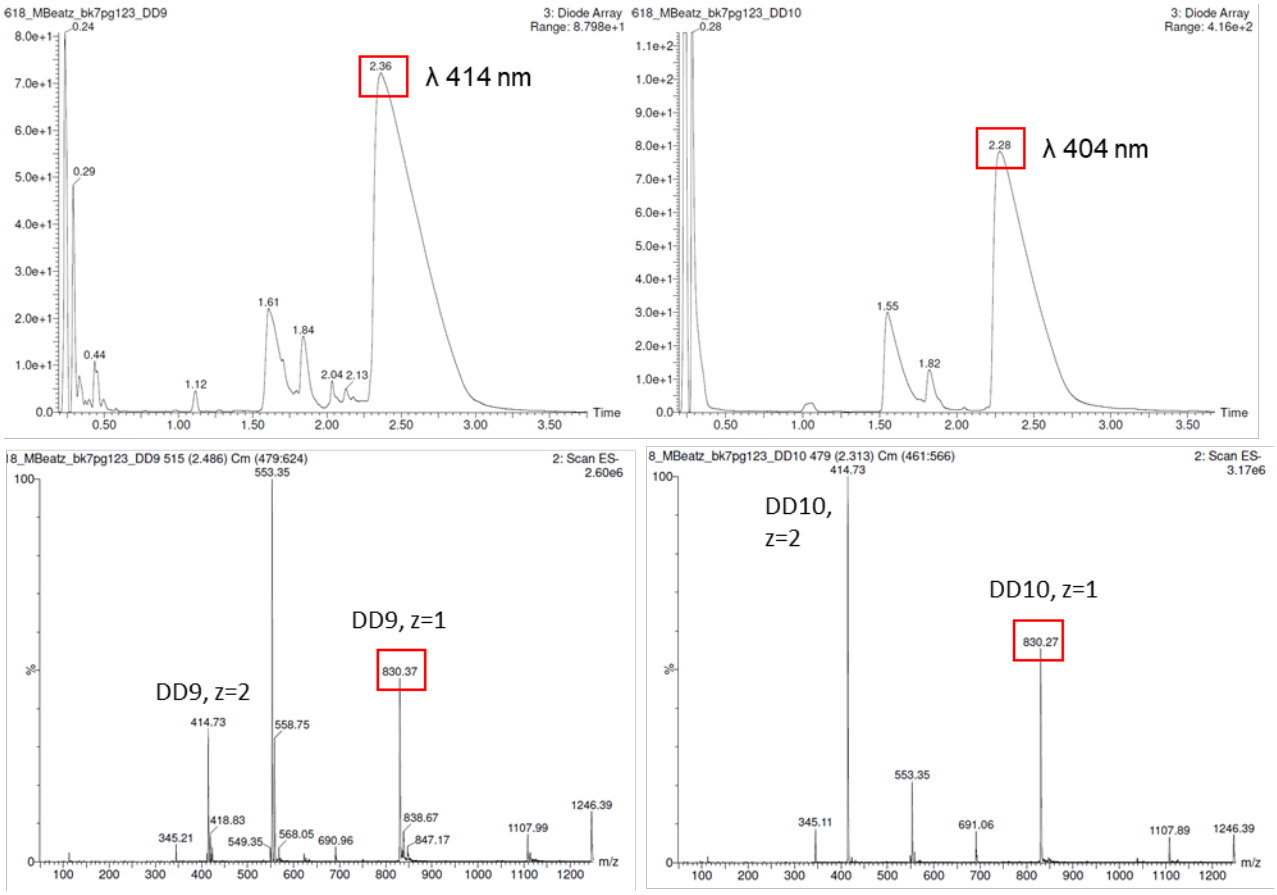

Figure S6. UPLC-MS traces confirm the partial synthesis of **DD9** (left) and **DD10** (right).

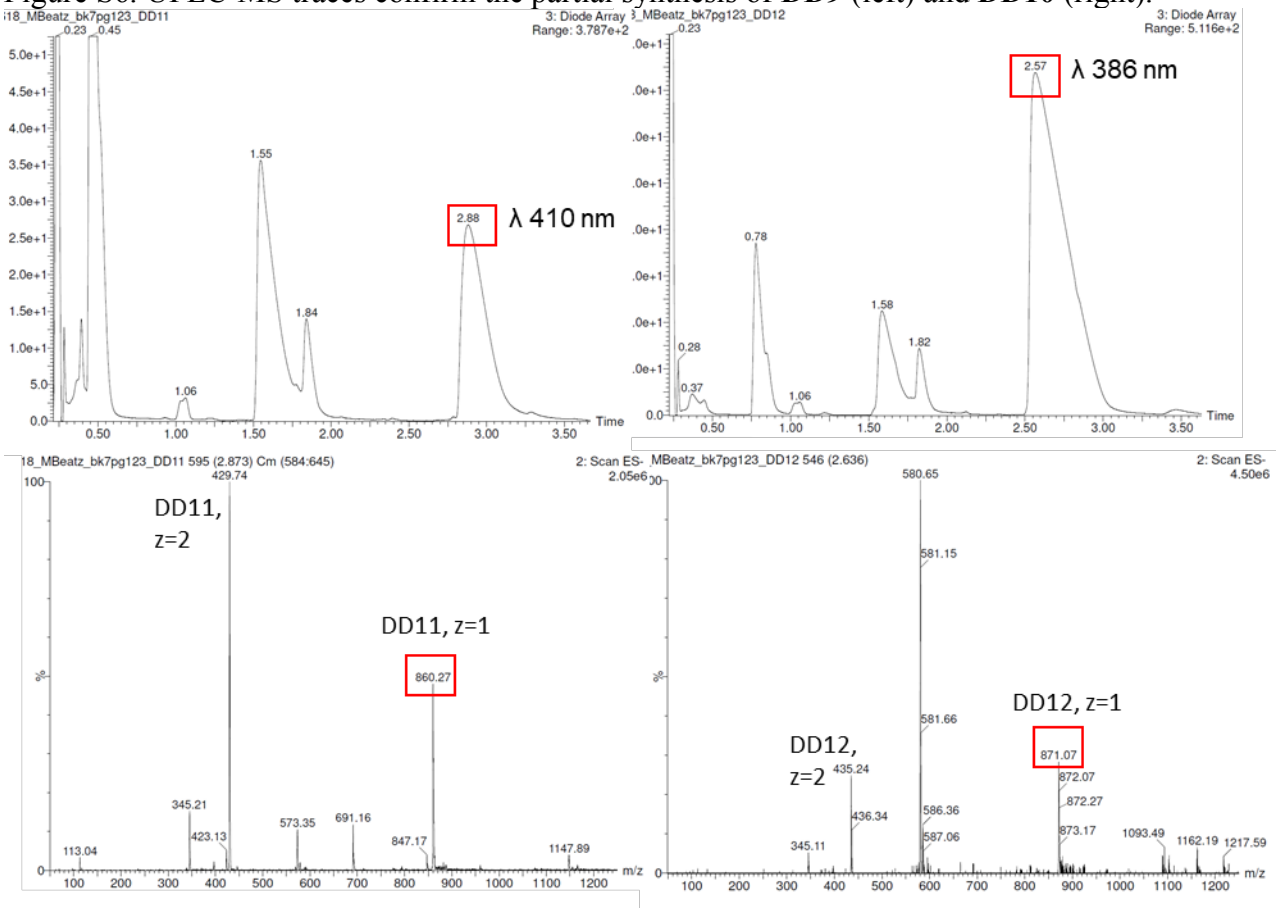

Figure S7. UPLC-MS traces confirm the partial synthesis of **DD11** (left) and **DD12** (right).

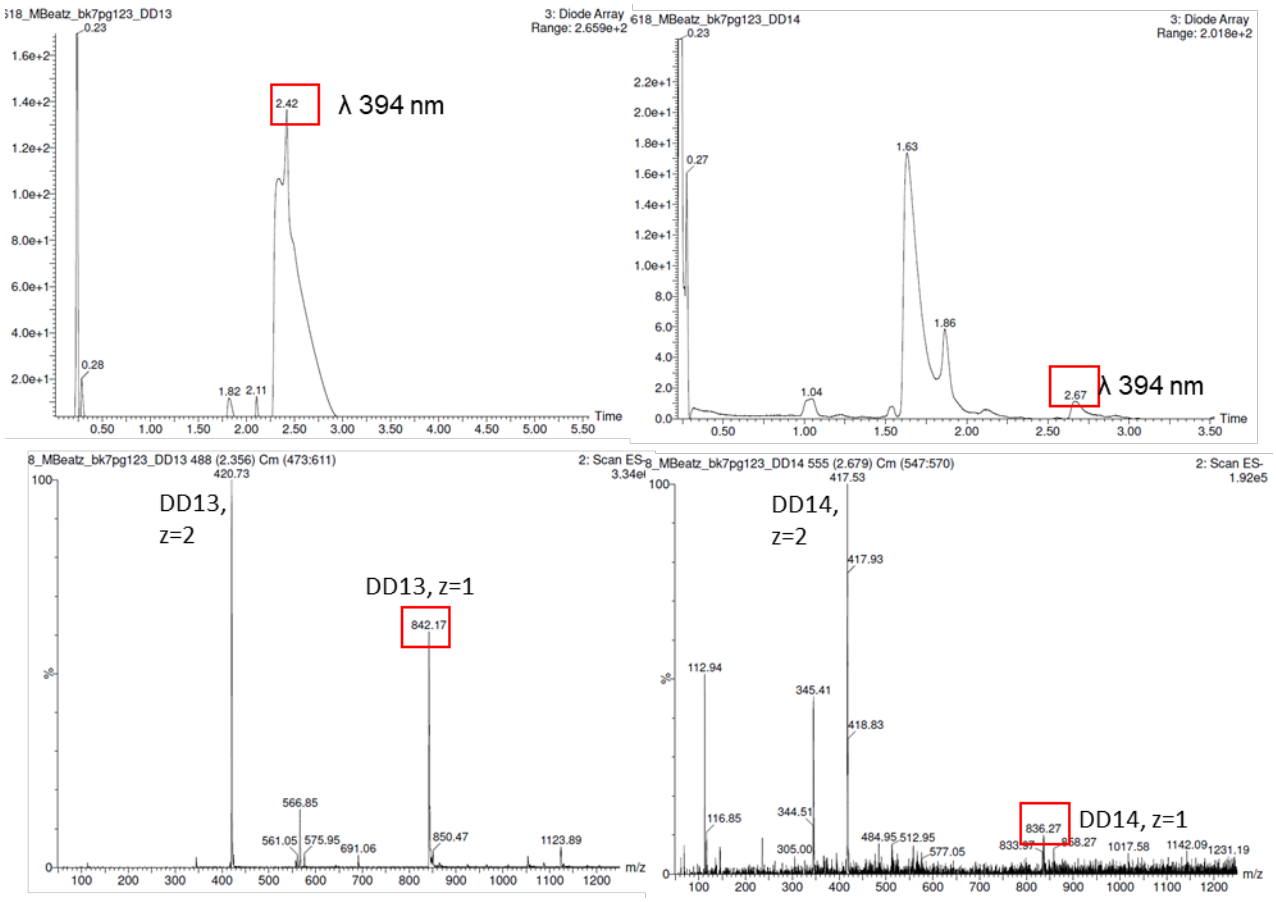

Figure S8. UPLC-MS traces confirm the nearly complete synthesis of **DD13** (left) and trace formation of **DD14** (right).

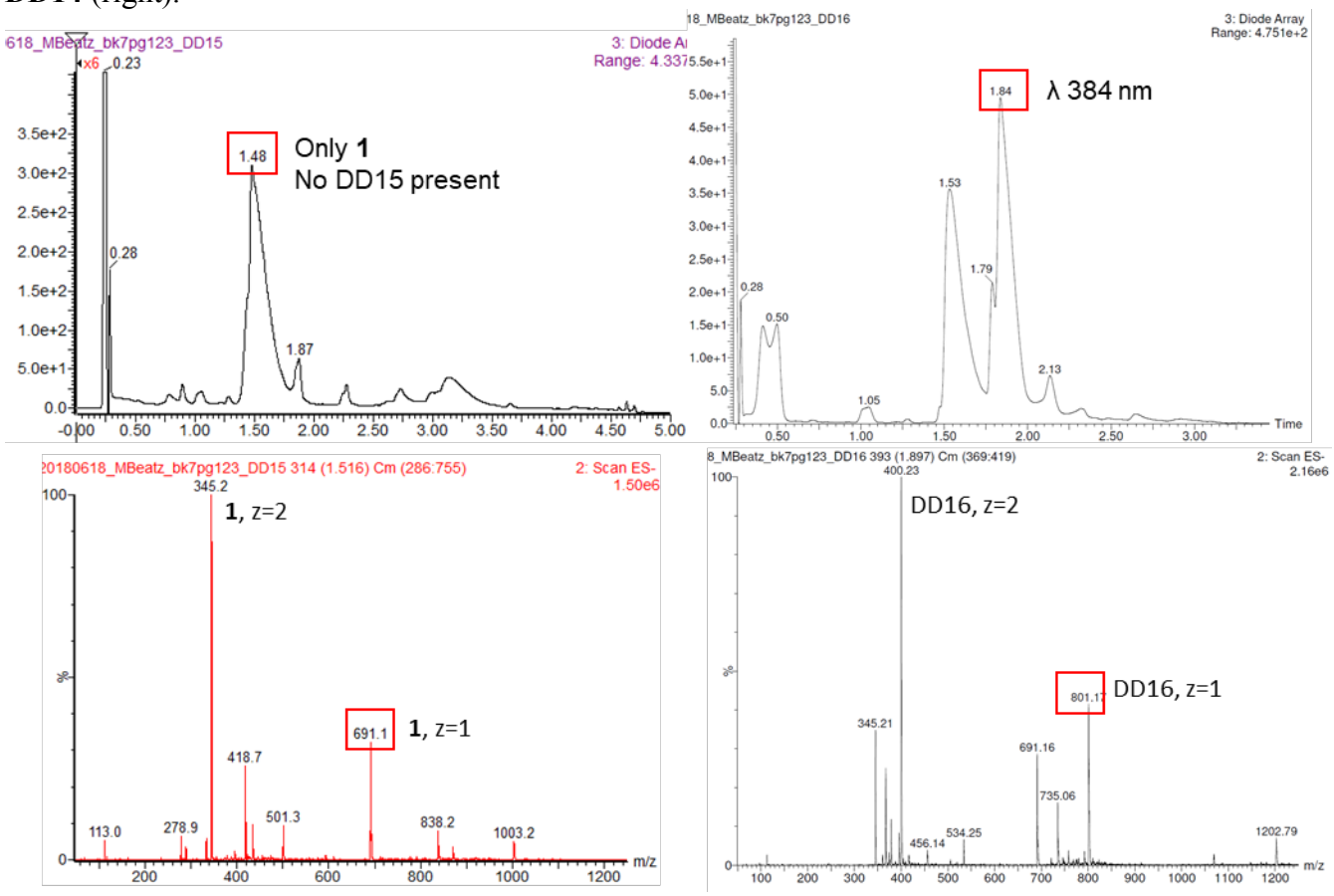

Figure S9. UPLC-MS traces show no conversion of **DD15** (left) and partial conversion of **DD16** (right).

6. ^{1}H NMR titrations with nicotine

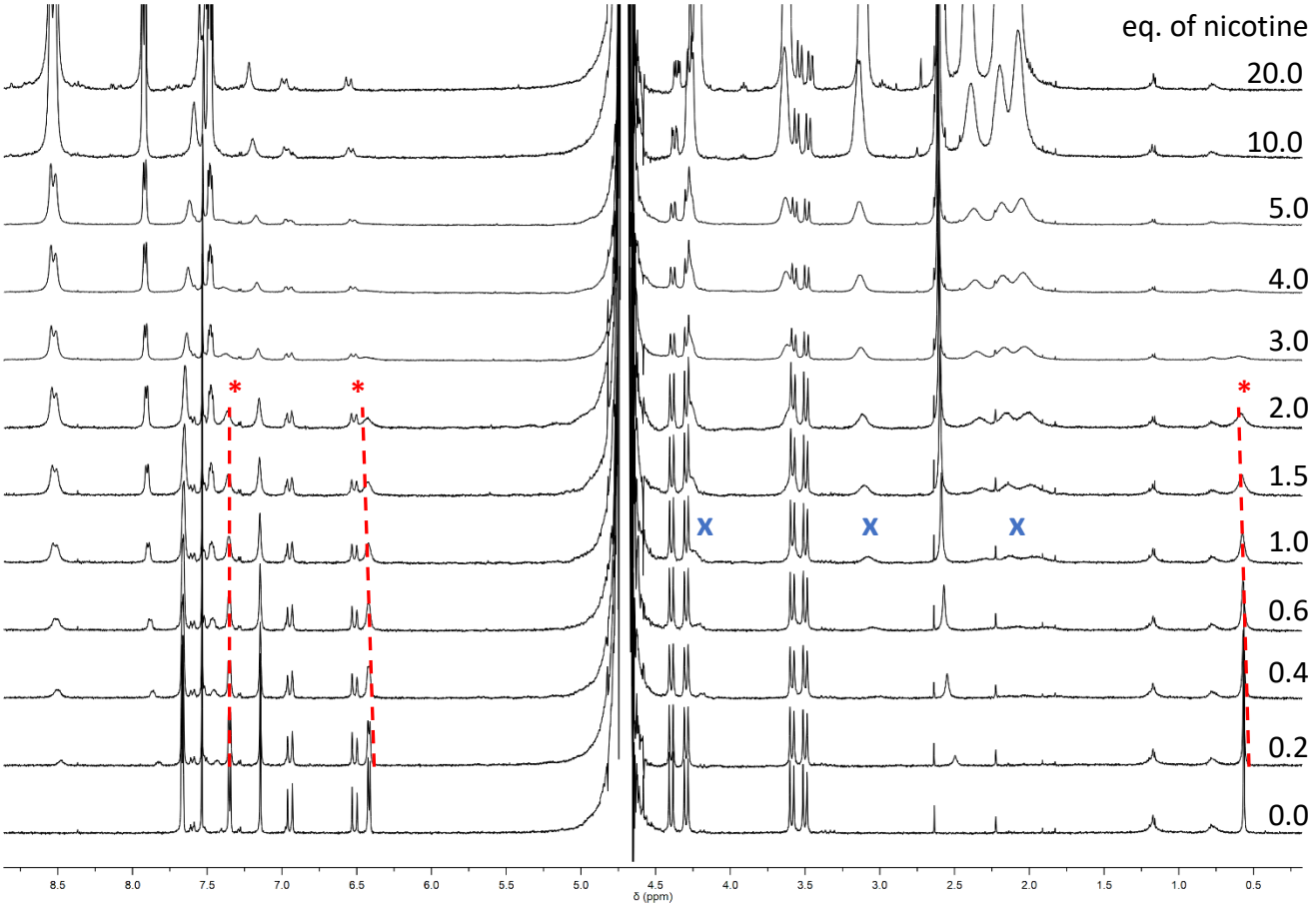

Figure S10. Nicotine titration (10 mM) into **DD1** (500 μM) shows broadening of resonances that support host-guest binding. The resonances of *N*-CH_3, ortho and meta pyridinium resonances on **DD1**, highlighted by red stars, begin to broaden upon the addition of nicotine. While pyrrolidine protons of nicotine, highlighted with blue cross, barely become visible at 1.0 eq and remain broad throughout the titration. Although resonances of a distinct **DD1**$_{monomer}$-nicotine complex are not present the broadening is evidence of two equilibria (dimer dissociation and nicotine complexation) occurring together in an intermediate timescale relative to the NMR experiment.

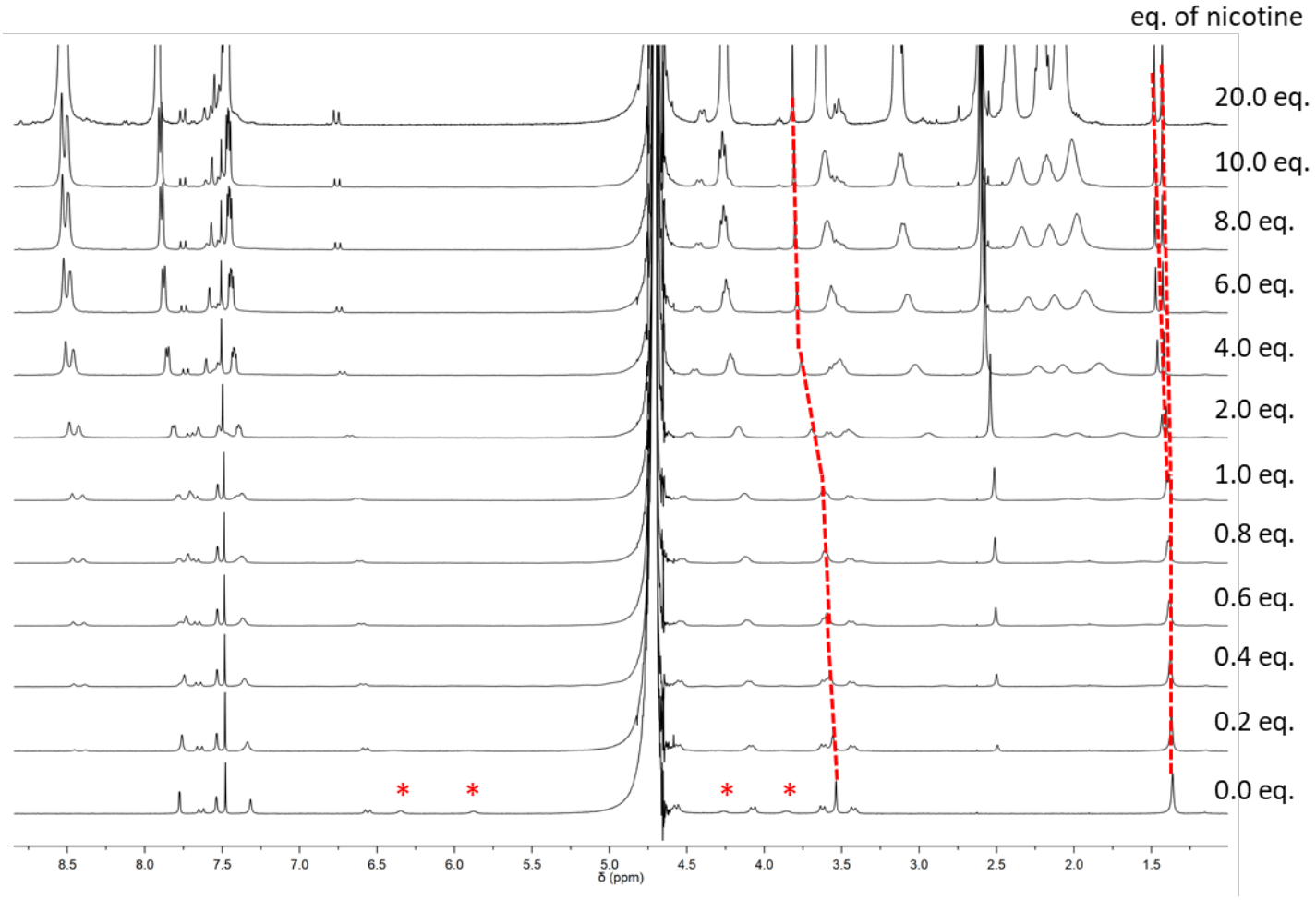

Figure S11. Nicotine titration (10 mM) into **DD4** (500 μM) shows shifts and broadening of resonances that support host-guest binding. The encapsulated aromatic indolinium protons on **DD4**, highlighted by red stars, broaden immediately upon the addition of nicotine. The methyl groups: *N*-CH_3 and the 3-dimethyl protons, can be followed with red dashed lines and are in fast exchange relative to the NMR timescale. The two equivalent dimethyl groups, found as a 6H singlet at 0.0 eq, split into two chemically inequivalent singlets upon the addition of nicotine.

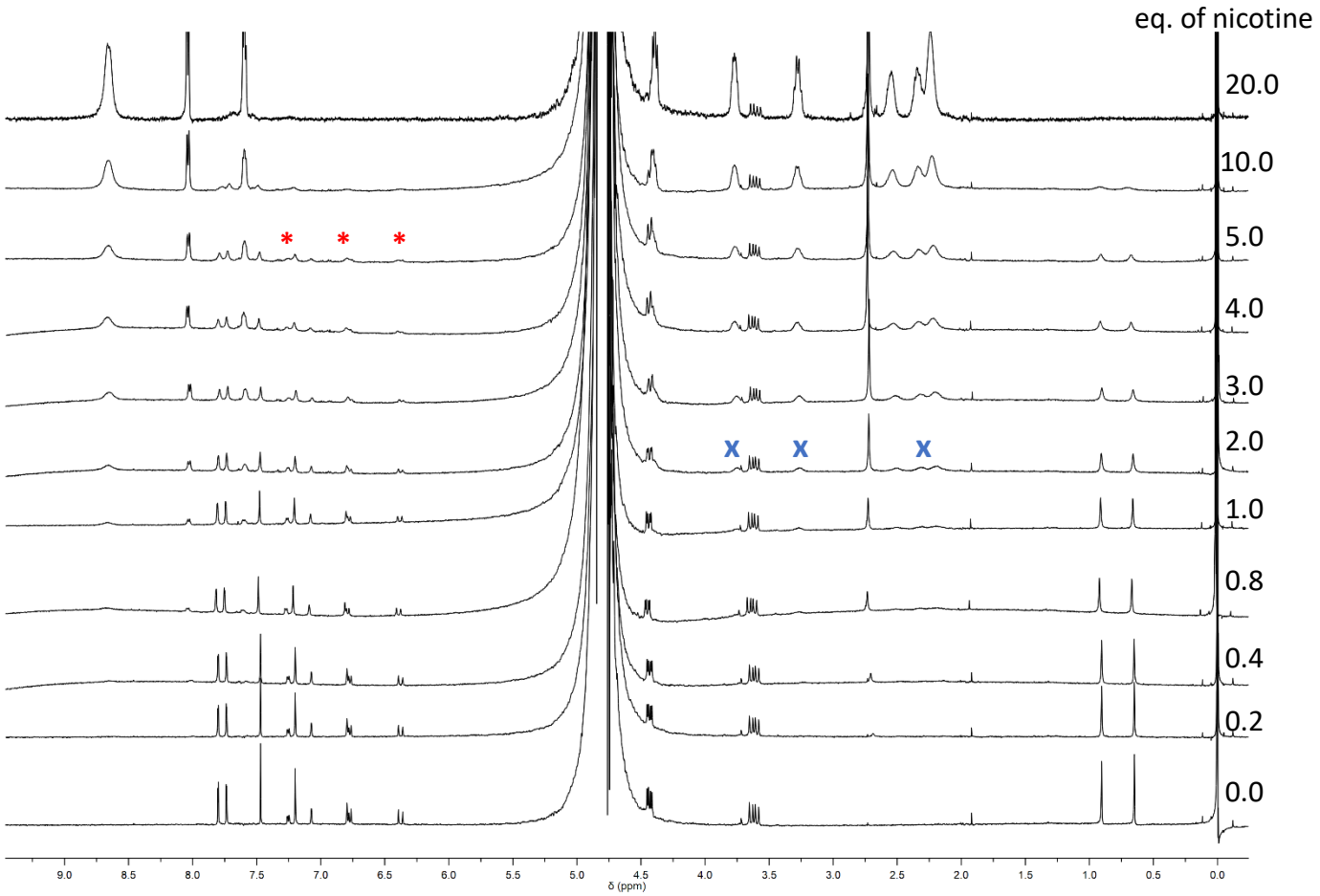

Figure S12. Nicotine titration (4 mM) into **DD8** (200 μM) shows broadening of resonances that supports host-guest binding. **DD8** resonances did not shift but only broadened completely into the baseline, indicated with red stars. Nicotine resonances began to appear at 2.0 eq. and remained broad throughout the titration.

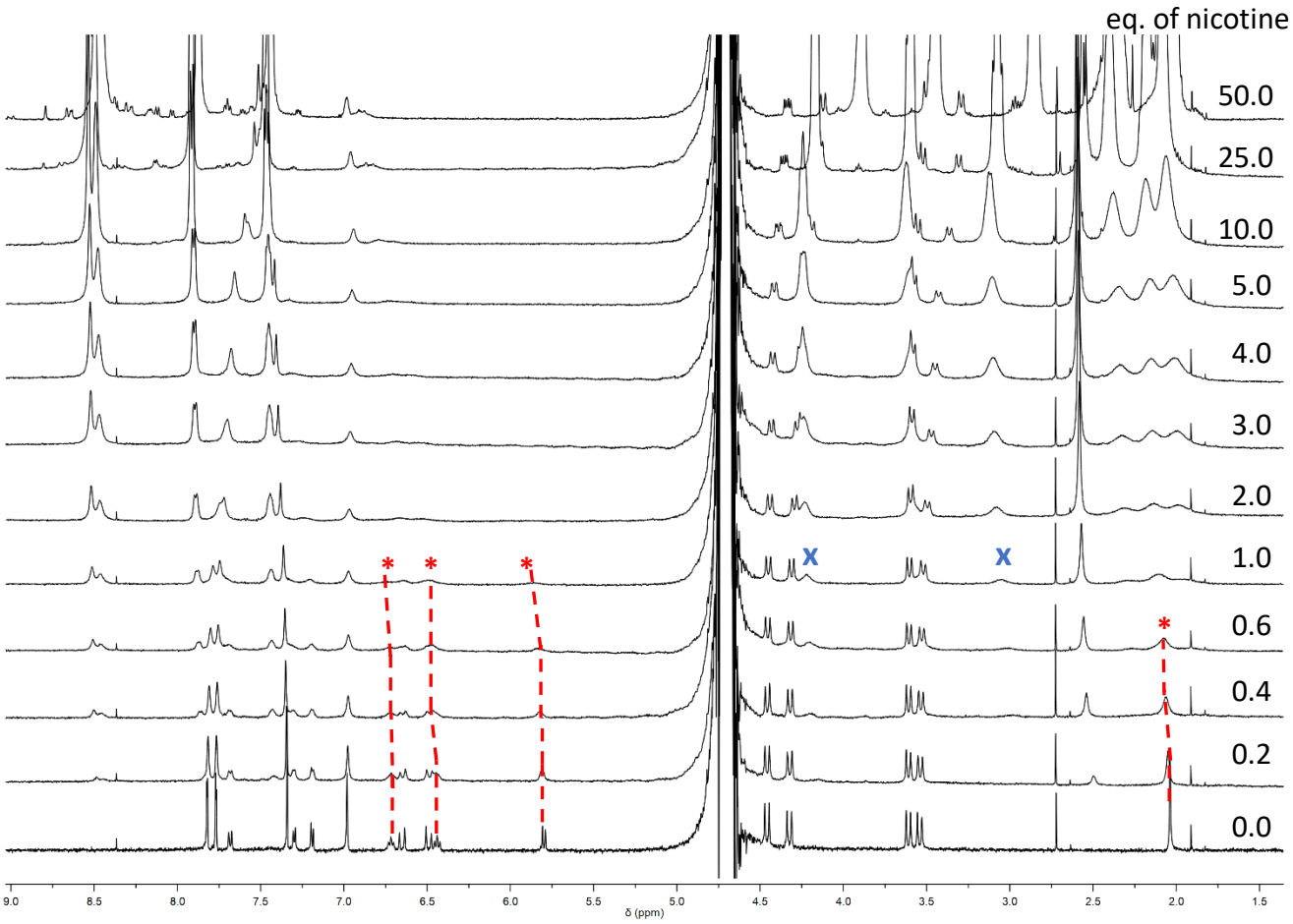

Figure S13. Nicotine titration (25 mM) into **DD9** (500 μM) shows shifts and broadening of resonances that support host-guest binding. **DD9** quinolinium and *N*-CH_3 resonances broadened and shifted downfield slightly (indicated with red stars and dashed lines) and eventually flattened into the baseline after 1.0 eq of nicotine was added. Nicotine pyrrolidine resonances appeared at 1.0 eq (marked with a blue cross) and remained broad throughout the titration.

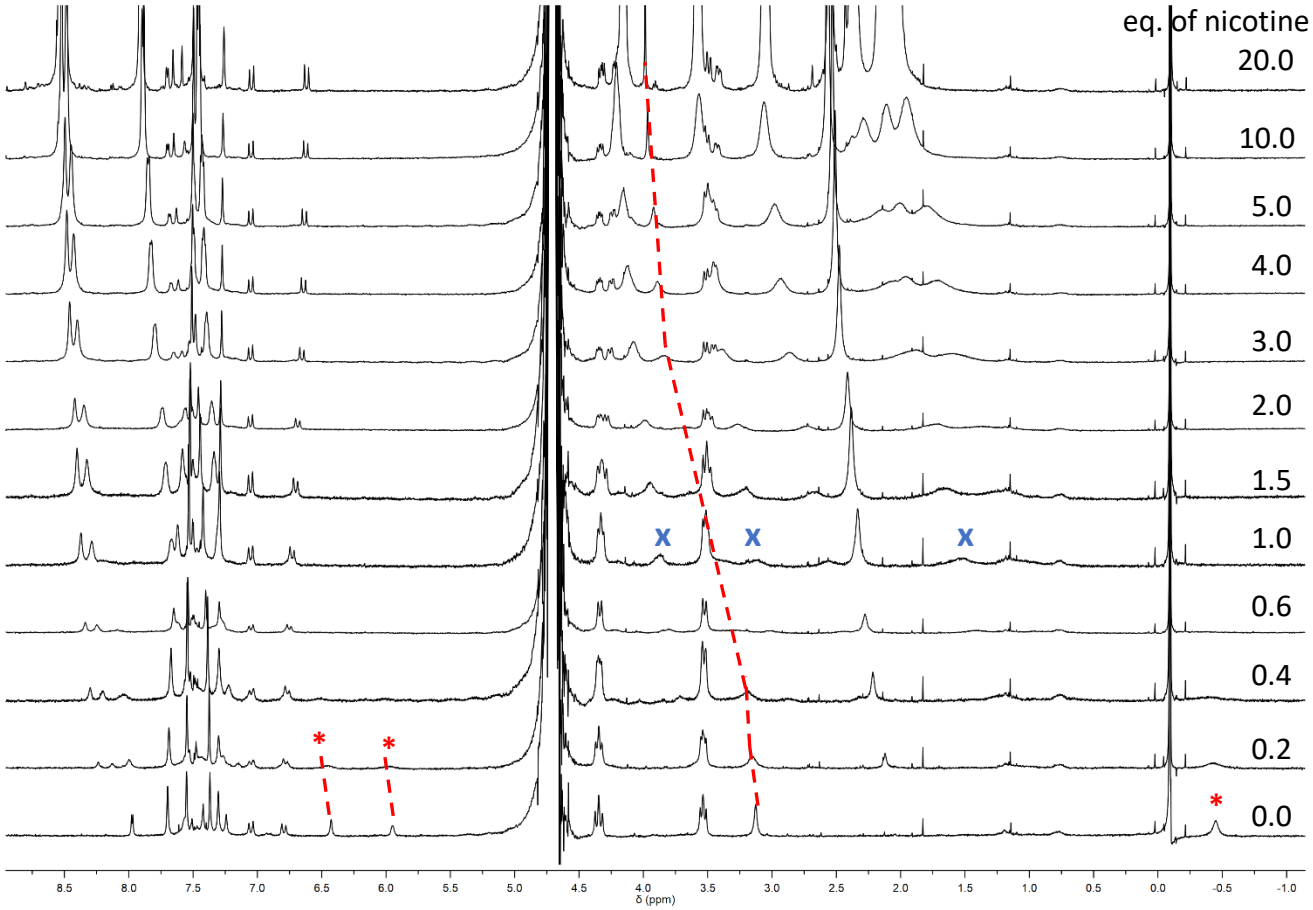

Figure S14. Nicotine titration (10 mM) into **DD12** (500 μM) shows shifts and broadening of resonances that support host-guest binding. The encapsulated aromatic pyridinium protons and 4'-CH_3 on **DD12**, highlighted by red stars, broaden immediately upon the addition of nicotine. However, the less shielded *N*-CH_3, can be followed with red dashed lines and is in fast exchange relative to the NMR timescale, shifting by 0.86 ppm. The nicotine pyrrolidine resonances appear as broad signals near 1.0 eq. and remain broad throughout the titration.

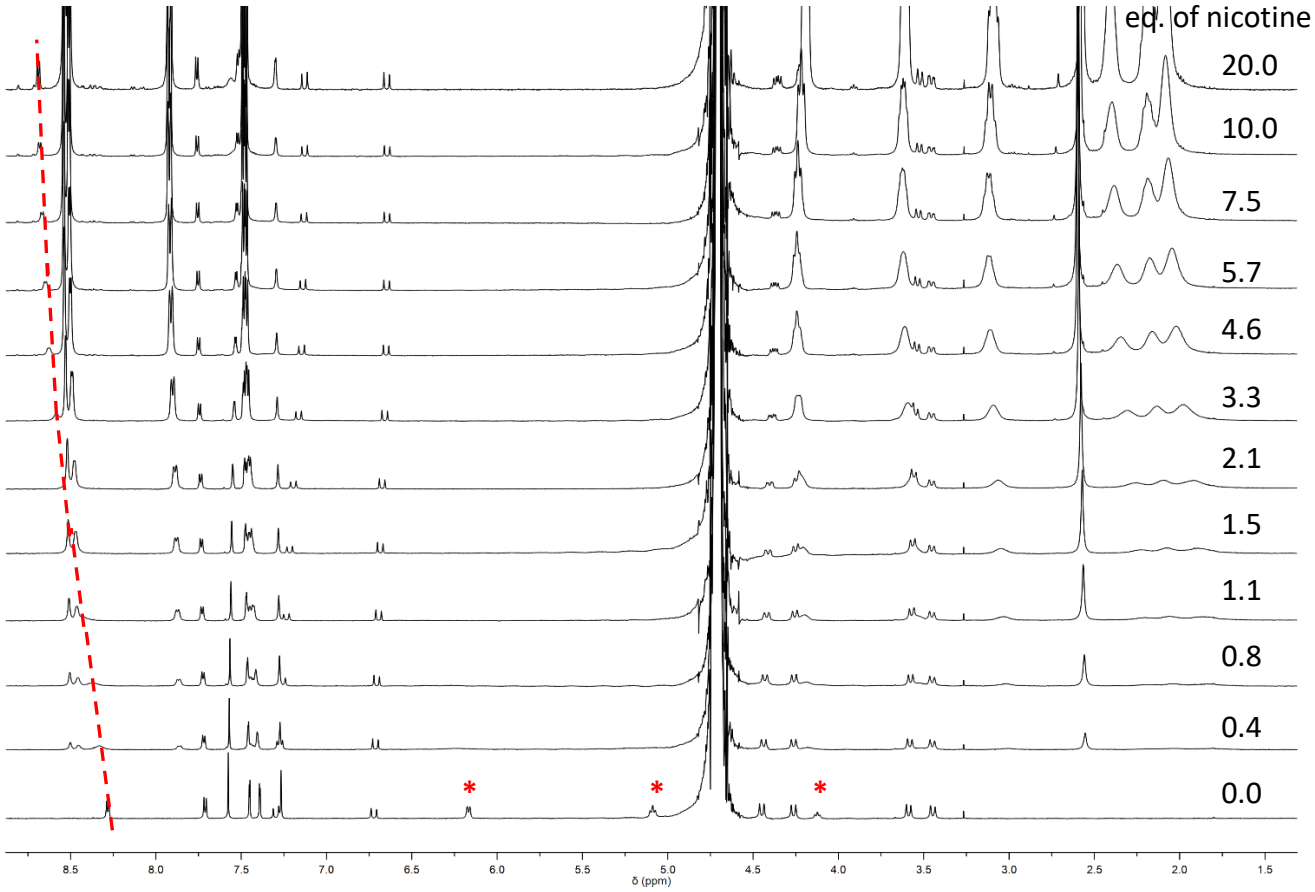

Figure S15. Nicotine titration (10 mM) into **DD13** (500 μM) shows shifts and broadening of resonances that support host-guest binding. The encapsulated *N*-phenyl protons on **DD13**, highlighted by red stars, broaden immediately upon the addition of nicotine. However, the less shielded *ortho*-pyridinium resonances, can be followed with red dashed lines in fast exchange relative to the NMR timescale, shifting by 0.42 ppm.

a. Pictures of DimerDyes with and without nicotine under conditions of NMR experiments

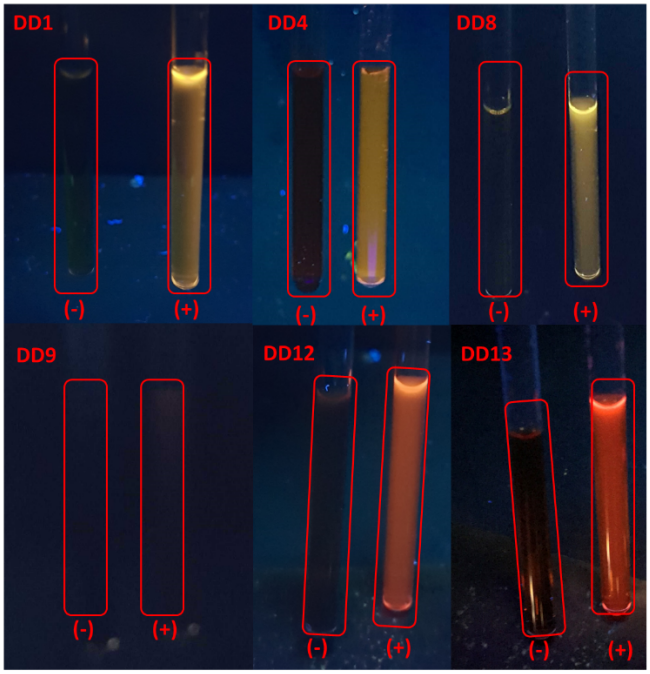

Figure S16. DimerDyes (500 μM) without nicotine (-) are not fluorescent. With addition of 10 mM nicotine (+), DimerDyes 1, 4, 8, 12 and 13 become fluorescent while **DD9** remains dark, as predicted by the screening of crude DD reaction mixtures. Each tube is irradiated with a hand-held UV lamp ($\lambda_{ex.}$ 364 nm ± 20 nm). Solutions are prepared in NaH_2PO_4/Na_2HPO_4 buffered D_2O, (50 mM, pD 7.4).

7. 1D DOSY calculations (1, DD4, DD4 + 20 eq. nicotine)

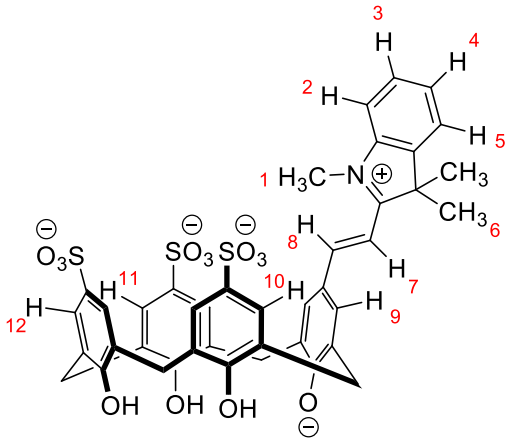

Table S3. Diffusion coefficients measured, and hydrodynamic radii calculated from indicated resonances in **DD4** from 1D DOSY.

Atom	D (m^2/s)	r (Å)
H8	1.944E-10	12.64
H7	1.986E-10	12.37
H2	1.99E-10	12.35
H1	1.952E-10	12.59
H6	1.924E-10	12.77

DD4 (4.34 mM) was NaH_2PO_4/Na_2HPO_4 (50 mM, pD 7.4) in D_2O. P1 = 8.35 µs, D1 = 18.75 s, δ = 1800 µs, Δ = 100 ms.

The average hydrodynamic radius of **DD4** (r_H) was calculated as 12.53 ± 0.15 Å and the average diffusion coefficient (D) is 1.96 x10^{-10} m^2/s.

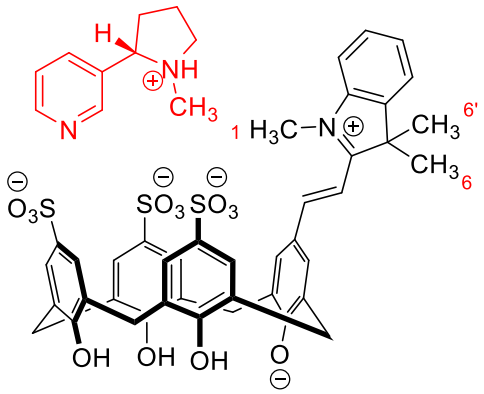

Table S4. Diffusion coefficients measured, and hydrodynamic radii calculated from indicated resonances in **DD4**—nicotine complex from 1D DOSY.

Atom	D (m^2/s)	r (Å)
H1	2.469E-10	9.95
H6	2.517E-10	9.76
H6'	2.58E-10	9.52

DD4 (500 µM) and nicotine (10 mM) were dissolved in NaH_2PO_4/Na_2HPO_4 (50 mM, pD 7.4) in D_2O. P1 = 8.35 µs, D1 = 10 s, δ = 1200 µs, Δ = 100 ms.

The average hydrodynamic radius of **DD4—nicotine complex** (r_H) was calculated as 9.74 ± 0.21 Å and the average diffusion coefficient (D) is 2.52 x10^{-10} m^2/s.

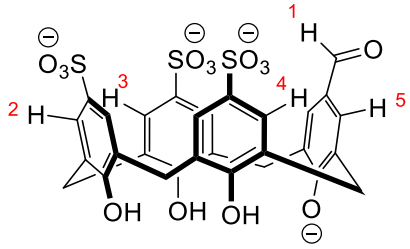

Table S5. Diffusion coefficients measured, and hydrodynamic radii calculated from indicated resonances in **1** from 1D DOSY.

Atom	D (m^2/s)	r (Å)
H1	3.3E-10	7.45
H2	3.28E-10	7.50
H3	3.27E-10	7.52
H4	3.29E-10	7.48
H5	3.28E-10	7.49

Compound **1** (4 mM) was dissolved in NaH_2PO_4/Na_2HPO_4 (100 mM, pD 7.4) in D_2O. P1 = 9.4 µs, D1 = 15.2 s, δ = 2500 µs, Δ = 50 ms.

The average hydrodynamic radius of **1** (r_H) was calculated as 7.49 ± 0.02 Å and the average diffusion coefficient (D) is 3.28 $x10^{-10}$ m^2/s.

8. Fluorescence titrations of DD4, DD8, DD9, DD12, DD13 with nicotine, MDMA and cocaine

All intensity values are plotted as the mean of duplicate experiments. Error bars corresponding to the standard deviation are present on all data points in all dose-response graphs (but in many cases are similar in size to the data point markers themselves). Spectra represent mean of duplicate experiments and are processed with second order smoothing function.

a. Nicotine

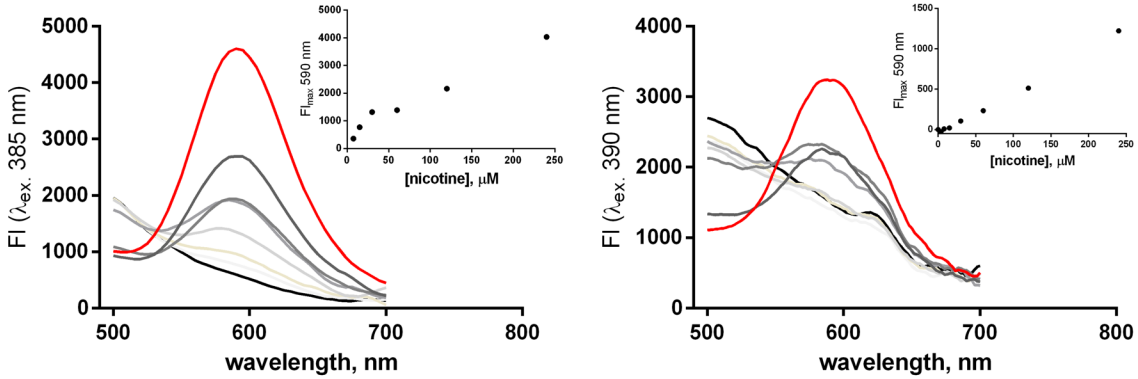

Figure S17. **DD1** turns-on fluorescence upon the addition of nicotine in buffered water and diluted saliva. Nicotine titration into **DD1** (12 μM) monitored by fluorescence spectroscopy in (left) NaH_2PO_4/Na_2HPO_4 buffered water (10 mM, pH 7.4, $\lambda_{ex.}$ = 385 nm) and in (right) diluted saliva (1:1, saliva:water, $\lambda_{ex.}$ = 390 nm) show **DD1** is capable of detecting nicotine in both media. Red line indicates maximum nicotine concentration = 240 μM and black line indicates no nicotine added. Insets show binding isotherms monitored at fluorescence maximum, $\lambda_{max.}$ = 590 nm in both saliva and water.

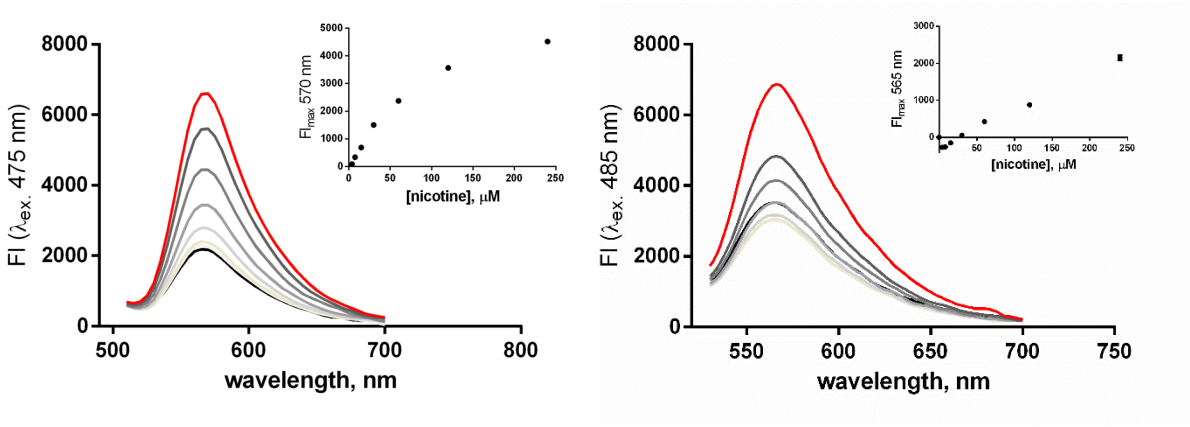

Figure S18. **DD4** turns-on fluorescence upon the addition of nicotine in buffered water and diluted saliva. Nicotine titration into **DD4** (12 μM) monitored by fluorescence spectroscopy in (left) NaH_2PO_4/Na_2HPO_4 buffered water (10 mM, pH 7.4, $\lambda_{ex.}$ = 475 nm) and in (right) diluted saliva (1:1, saliva:water, $\lambda_{ex.}$ = 485 nm), show **DD4** is capable of detecting nicotine in both media. Red line indicates maximum nicotine concentration = 240 μM and black line indicates no nicotine added. Insets show binding isotherms monitored at fluorescence maximum, $\lambda_{max.}$ = 570 nm in buffered water and $\lambda_{max.}$ = 585 nm in diluted saliva.

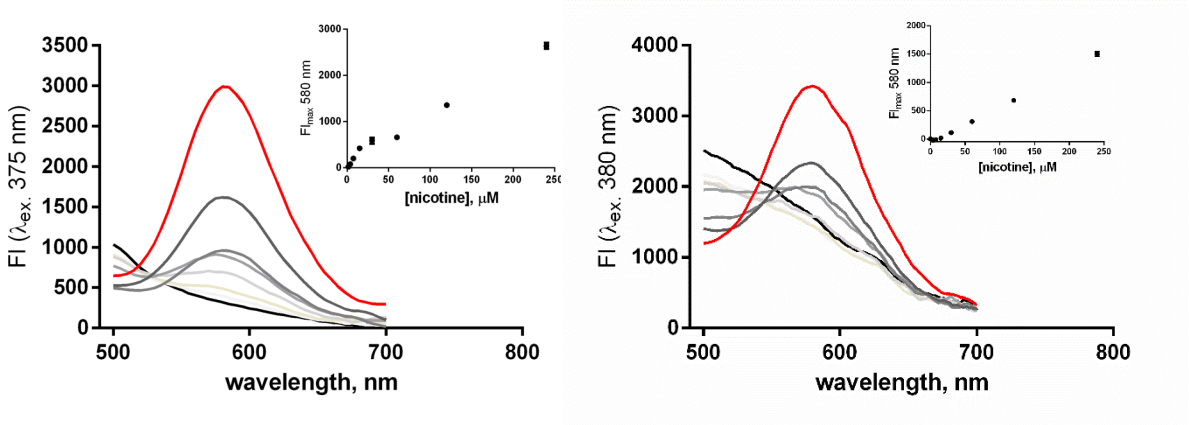

Figure S19. **DD8** turns-on fluorescence upon the addition of nicotine in buffered water and diluted saliva. Nicotine titration into **DD8** (12 μM) monitored by fluorescence spectroscopy in (left) NaH_2PO_4/Na_2HPO_4 buffered water (10 mM, pH 7.4, $\lambda_{ex.}$ = 375 nm) and in (right) diluted saliva (1:1, saliva:water, $\lambda_{ex.}$ = 380 nm) show **DD8** is capable of detecting nicotine in both media. Red line indicates maximum nicotine concentration = 240 μM and black line indicates no nicotine added. Insets show binding isotherms monitored at fluorescence maximum, $\lambda_{max.}$ = 580 nm in both buffered water and diluted saliva.

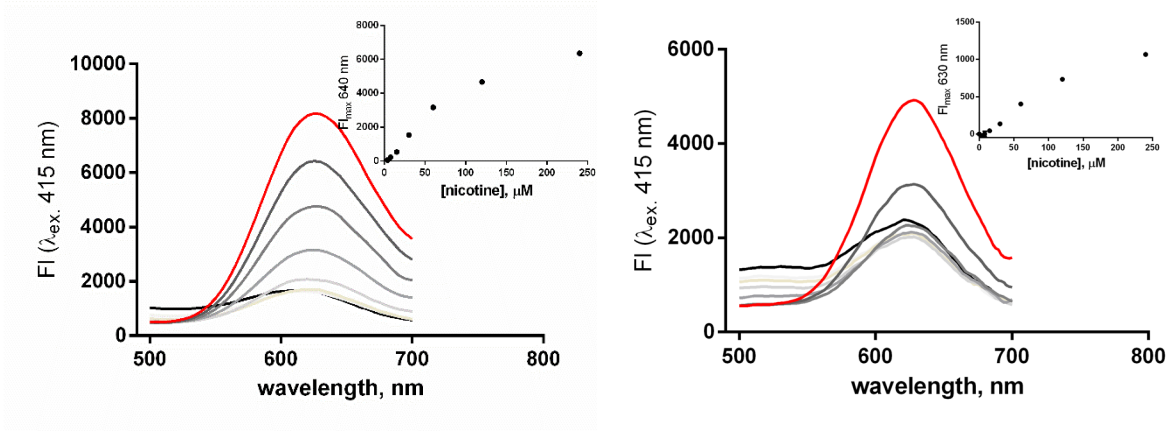

Figure S20. **DD12** turns-on fluorescence upon the addition of nicotine in buffered water and diluted saliva. Nicotine titration into **DD12** (12 μM) monitored by fluorescence spectroscopy in (left) NaH_2PO_4/Na_2HPO_4 buffered water (10 mM, pH 7.4, $\lambda_{ex.}$ = 415 nm) and in (right) diluted saliva (1:1, saliva:water, $\lambda_{ex.}$ = 415 nm) show **DD12** is capable of detecting nicotine in both media. Red line indicates maximum nicotine concentration = 240 μM and black line indicates no nicotine added. Insets show binding isotherms monitored at fluorescence maximum, $\lambda_{max.}$ = 640 nm in both buffered water and diluted saliva.

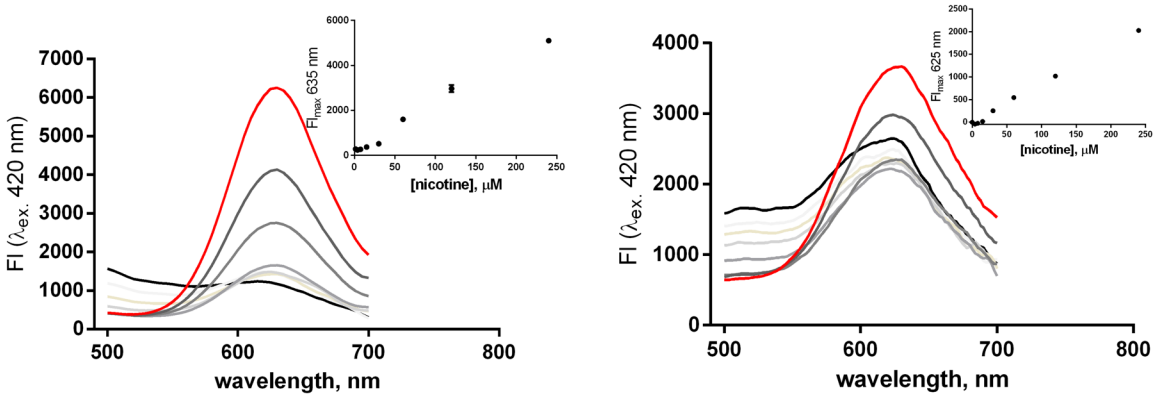

Figure S21. **DD13** turns-on fluorescence upon the addition of nicotine in buffered water and diluted saliva. Nicotine titration into **DD13** (12 μM) monitored by fluorescence spectroscopy in (left) NaH_2PO_4/Na_2HPO_4 buffered water (10 mM, pH 7.4, $\lambda_{ex.}$ = 420 nm) and in (right) diluted saliva (1:1, saliva:water, $\lambda_{ex.}$ = 420 nm) show **DD12** is capable of detecting nicotine in both media. Red line indicates maximum nicotine concentration = 240 μM and black line indicates no nicotine added. Insets show binding isotherms monitored at fluorescence maximum, $\lambda_{max.}$ = 635 nm in buffered water and $\lambda_{max.}$ = 625 nm in diluted saliva.

b. MDMA

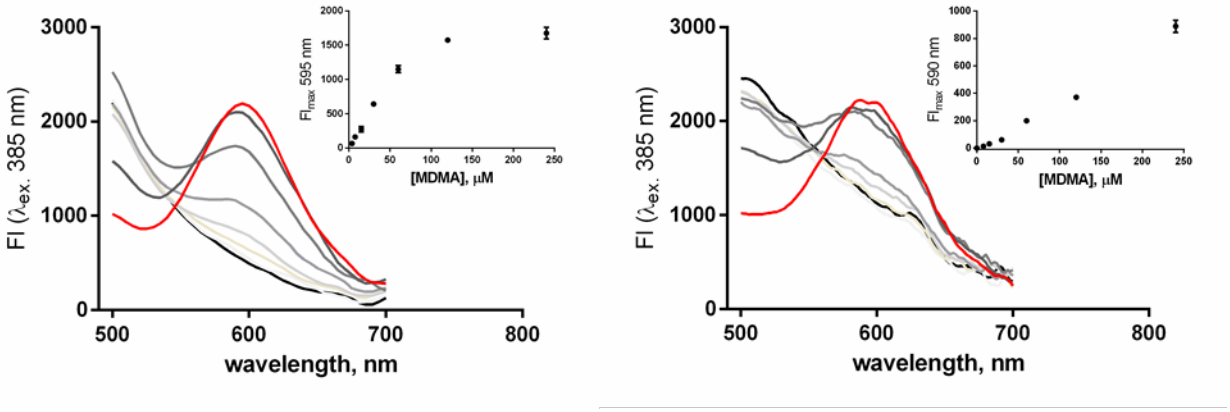

Figure S22. **DD1** turns-on fluorescence upon the addition of MDMA in buffered water and diluted saliva. MDMA titration into **DD1** (12 μM) monitored by fluorescence spectroscopy in (left) NaH_2PO_4/Na_2HPO_4 buffered water (10 mM, pH 7.4, $\lambda_{ex.}$ = 385 nm) and in (right) diluted saliva (1:1, saliva:water, $\lambda_{ex.}$ = 385 nm) show **DD1** is capable of detecting MDMA in both media. Red line indicates maximum MDMA concentration = 240 μM and black line indicates no MDMA added. Insets show binding isotherms monitored at fluorescence maximum, $\lambda_{max.}$ = 595 nm in buffered water and $\lambda_{max.}$ = 590 nm in diluted saliva.

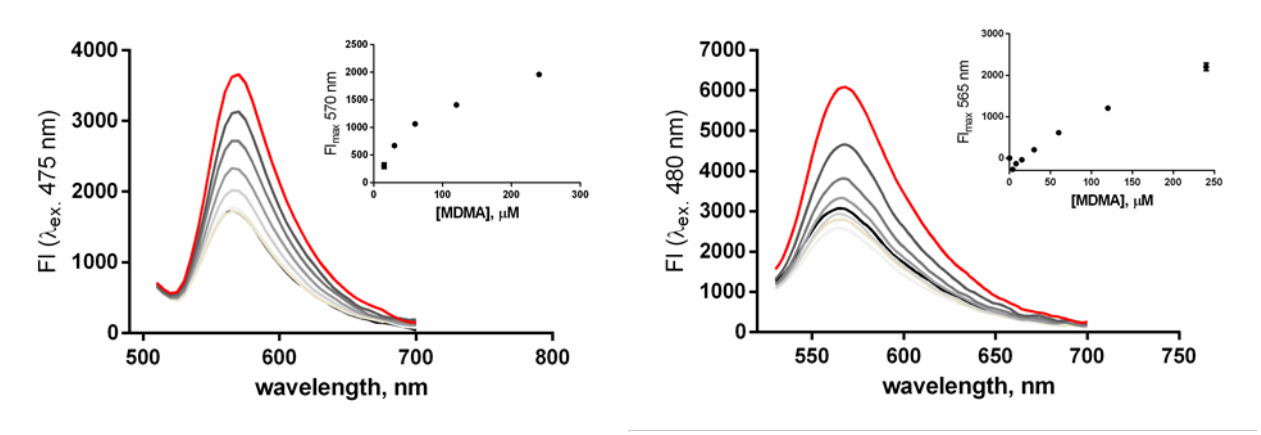

Figure S23. **DD4** turns-on fluorescence upon the addition of MDMA in buffered water and diluted saliva. MDMA titration into **DD4** (12 μM) monitored by fluorescence spectroscopy in (left) NaH_2PO_4/Na_2HPO_4 buffered water (10 mM, pH 7.4, $\lambda_{ex.}$ = 475 nm) and in (right) diluted saliva (1:1, saliva:water, $\lambda_{ex.}$ = 480 nm) show **DD4** is capable of detecting MDMA in both media. Red line indicates maximum MDMA concentration = 240 μM and black line indicates no MDMA added. Insets show binding isotherms monitored at fluorescence maximum, $\lambda_{max.}$ = 595 nm in buffered water and $\lambda_{max.}$ = 590 nm in diluted saliva.

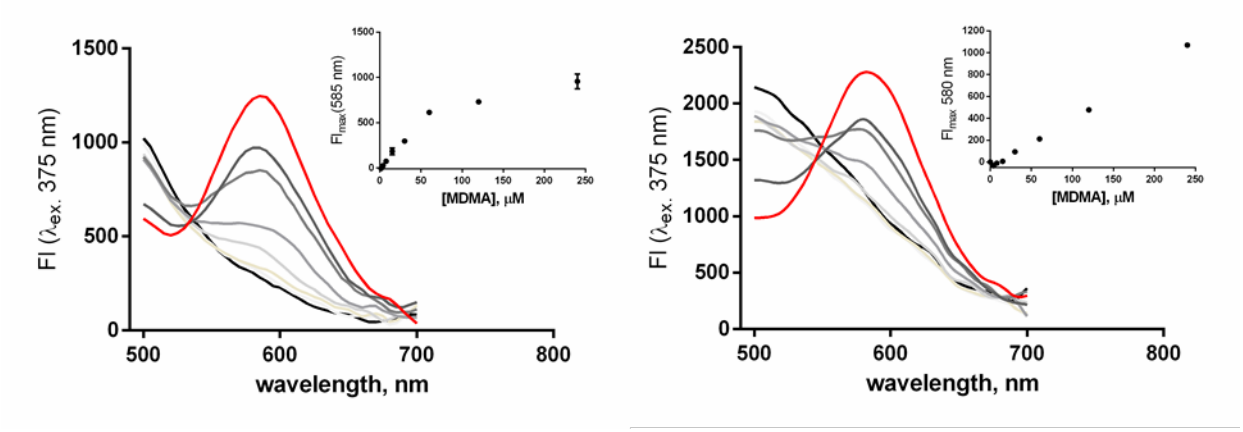

Figure S24. **DD8** turns-on fluorescence upon the addition of MDMA in buffered water and diluted saliva. MDMA titration into **DD8** (12 μM) monitored by fluorescence spectroscopy in (left) NaH_2PO_4/Na_2HPO_4 buffered water (10 mM, pH 7.4, $\lambda_{ex.}$ = 375 nm) and in (right) diluted saliva (1:1, saliva:water, $\lambda_{ex.}$ = 375 nm) show **DD8** is capable of detecting MDMA in both media. Red line indicates maximum MDMA concentration = 240 μM and black line indicates no MDMA added. Insets show binding isotherms monitored at fluorescence maximum, $\lambda_{max.}$ = 585 nm in buffered water and $\lambda_{max.}$ = 580 nm in diluted saliva.

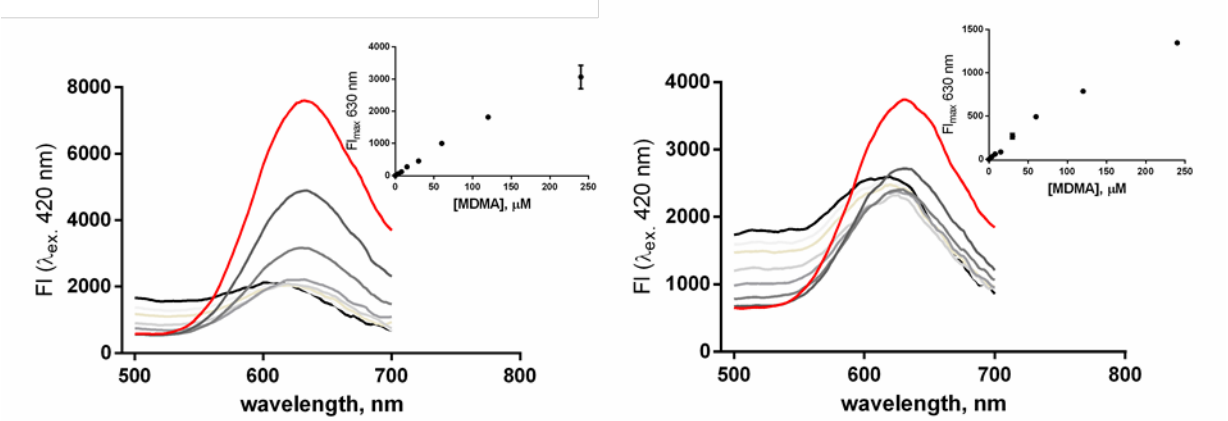

Figure S25. **DD12** turns-on fluorescence upon the addition of MDMA in buffered water and diluted saliva. MDMA titration into **DD12** (12 μM) monitored by fluorescence spectroscopy in (left) NaH_2PO_4/Na_2HPO_4 buffered water (10 mM, pH 7.4, $\lambda_{ex.}$ = 420 nm) and in (right) diluted saliva (1:1, saliva:water, $\lambda_{ex.}$ = 420 nm) show **DD12** is capable of detecting MDMA in both media. Red line indicates maximum MDMA concentration = 240 μM and black line indicates no MDMA added. Insets show binding isotherms monitored at fluorescence maximum, $\lambda_{max.}$ = 630 nm in both buffered water and in diluted saliva.

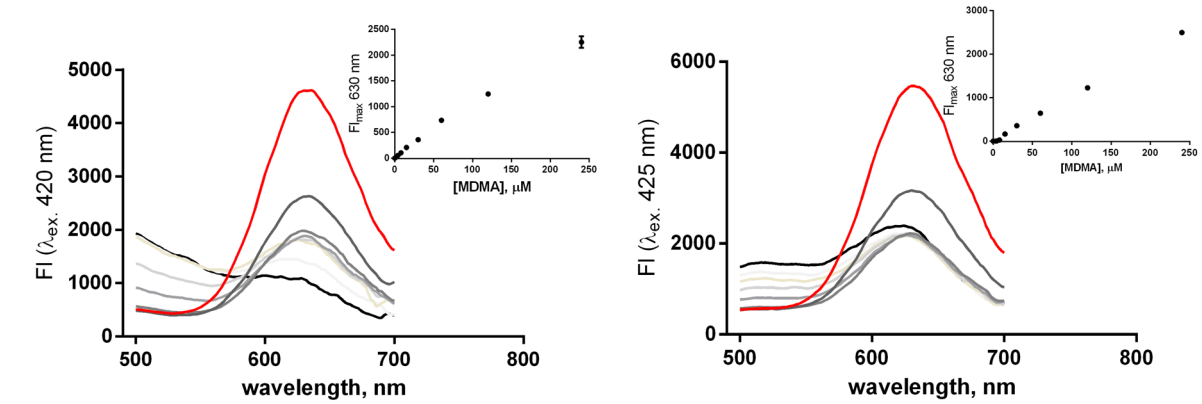

Figure S26. **DD13** turns-on fluorescence upon the addition of MDMA in buffered water and diluted saliva. MDMA titration into **DD13** (12 μM) monitored by fluorescence spectroscopy in (left) NaH_2PO_4/Na_2HPO_4 buffered water (10 mM, pH 7.4, $\lambda_{ex.}$ = 420 nm) and in (right) diluted saliva (1:1, saliva:water, $\lambda_{ex.}$ = 420 nm) show **DD13** is capable of detecting MDMA in both media. Red line indicates maximum MDMA concentration = 240 μM and black line indicates no MDMA added. Insets show binding isotherms monitored at fluorescence maximum, $\lambda_{max.}$ = 630 nm in both buffered water and in diluted saliva.

c. Cocaine

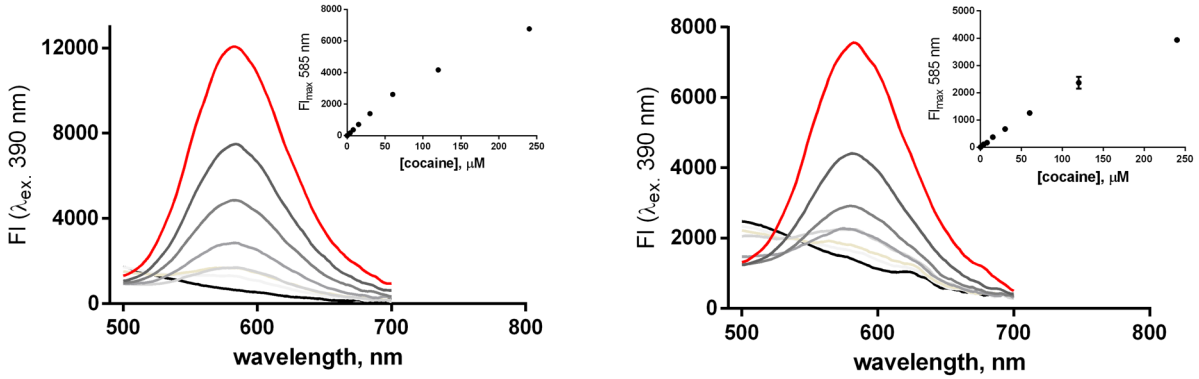

Figure S27. **DD1** turns-on fluorescence upon the addition of cocaine in buffered water and diluted saliva. Cocaine titration into **DD1** (12 μM) monitored by fluorescence spectroscopy in (left) NaH_2PO_4/Na_2HPO_4 buffered water (10 mM, pH 7.4, $\lambda_{ex.}$ = 390 nm) and in (right) diluted saliva (1:1, saliva:water, $\lambda_{ex.}$ = 390 nm) show **DD1** is capable of detecting cocaine in both media. Red line indicates maximum cocaine concentration = 240 μM and black line indicates no cocaine added. Insets show binding isotherms monitored at fluorescence maximum, $\lambda_{max.}$ = 585 nm in both buffered water and in diluted saliva.

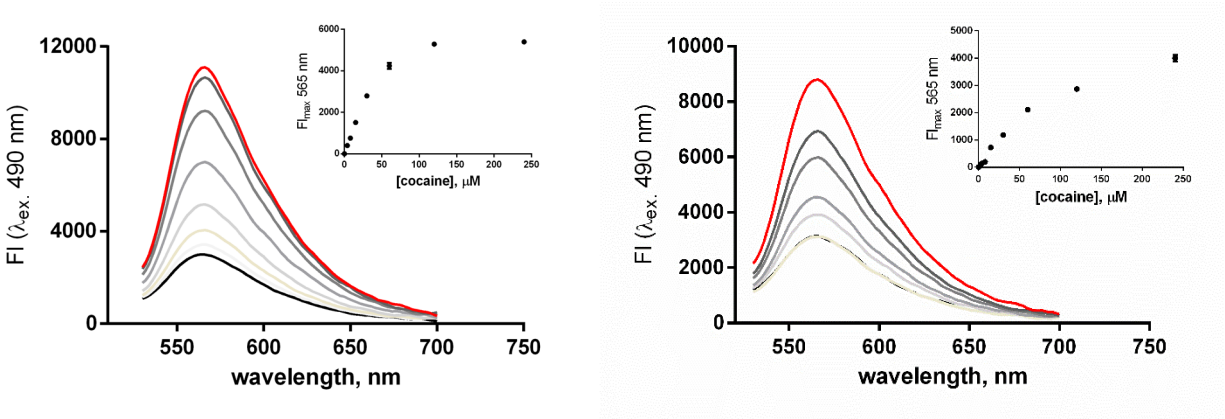

Figure S28. **DD4** turns-on fluorescence upon the addition of cocaine in buffered water and diluted saliva. Cocaine titration into **DD4** (12 μM) monitored by fluorescence spectroscopy in (left) NaH_2PO_4/Na_2HPO_4 buffered water (10 mM, pH 7.4, $\lambda_{ex.}$ = 490 nm) and in (right) diluted saliva (1:1, saliva:water, $\lambda_{ex.}$ = 490 nm) show **DD4** is capable of detecting cocaine in both media. Red line indicates maximum cocaine concentration = 240 μM and black line indicates no cocaine added. Insets show binding isotherms monitored at fluorescence maximum, $\lambda_{max.}$ = 565 nm in both buffered water and in diluted saliva.

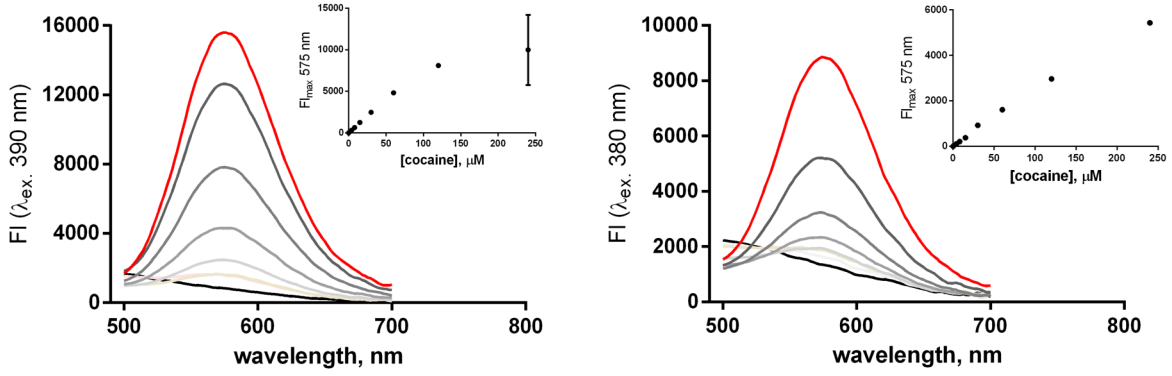

Figure S29. **DD8** turns-on fluorescence upon the addition of cocaine in buffered water and diluted saliva. Cocaine titration into **DD8** (12 μM) monitored by fluorescence spectroscopy in (left) NaH_2PO_4/Na_2HPO_4 buffered water (10 mM, pH 7.4, $\lambda_{ex.}$ = 390 nm) and in (right) diluted saliva (1:1, saliva:water, $\lambda_{ex.}$ = 380 nm) show **DD4** is capable of detecting cocaine in both media. Red line indicates maximum cocaine concentration = 240 μM and black line indicates no cocaine added. Insets show binding isotherms monitored at fluorescence maximum, $\lambda_{max.}$ = 575 nm in both buffered water and in diluted saliva.

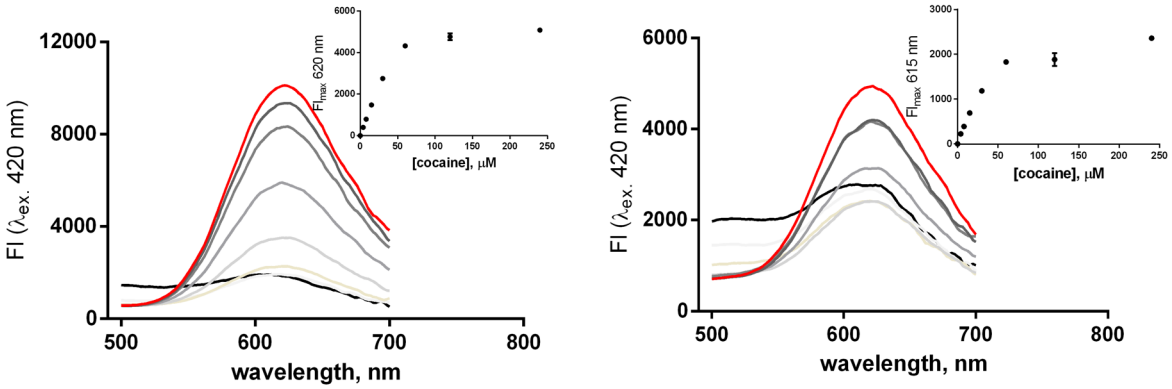

Figure S30. **DD12** turns-on fluorescence upon the addition of cocaine in buffered water and diluted saliva. Cocaine titration into **DD12** (12 μM) monitored by fluorescence spectroscopy in (left) NaH_2PO_4/Na_2HPO_4 buffered water (10 mM, pH 7.4, $\lambda_{ex.}$ = 420 nm) and in (right) diluted saliva (1:1, saliva:water, $\lambda_{ex.}$ = 420 nm) show **DD12** is capable of detecting cocaine in both media. Red line indicates maximum cocaine concentration = 240 μM and black line indicates no cocaine added. Insets show binding isotherms monitored at fluorescence maximum, $\lambda_{max.}$ = 620 nm in buffered water and $\lambda_{max.}$ = 615 nm in diluted saliva.

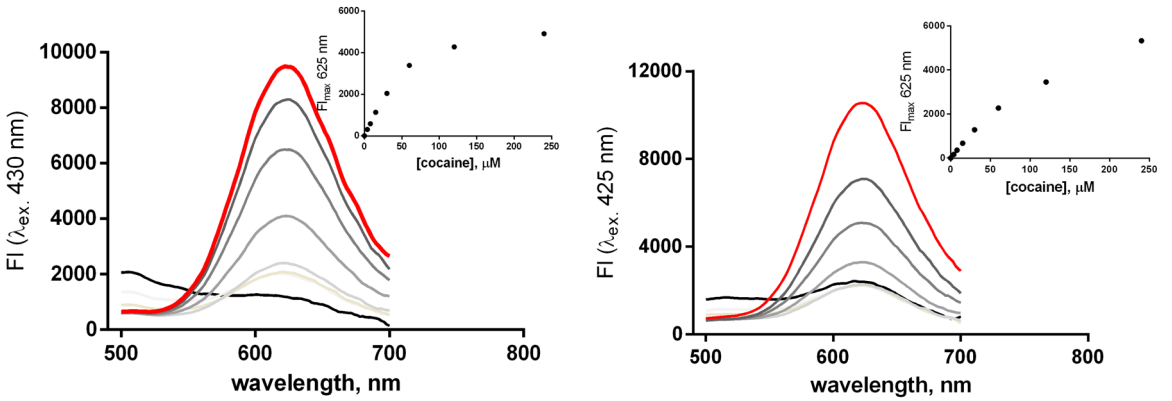

Figure S31. **DD13** turns-on fluorescence upon the addition of cocaine in buffered water and diluted saliva. Cocaine titration into **DD13** (12 μM) monitored by fluorescence spectroscopy in (left) NaH_2PO_4/Na_2HPO_4 buffered water (10 mM, pH 7.4, $\lambda_{ex.}$ = 430 nm) and in (right) diluted saliva (1:1, saliva:water, $\lambda_{ex.}$ = 425 nm) show **DD13** is capable of detecting cocaine in both media. Red line indicates maximum cocaine concentration = 240 μM and black line indicates no cocaine added. Insets show binding isotherms monitored at fluorescence maximum, $\lambda_{max.}$ = 625 nm in both buffered water and in diluted saliva.

9. Limits of Detection

Limits of detection were found through the linear regression of each data set and calculating:
LOD = σ/slope*3.3
Where, σ and slope are the standard deviation and slope obtained from the regression line
All LOD were measured with purified **DD**s, [**DD**] = 12 μM.

Table S6. Limits of detection (LOD) determined of each DimerDye for nicotine, MDMA and cocaine in sodium phosphate buffer

	Nicotine			MDMA			Cocaine		
	σ	SLOPE	LOD (μM)	σ	SLOPE	LOD (μM)	σ	SLOPE	LOD (μM)
DD1	45.91	43.42	3.489245	16.2	19.65	2.720611	12.87	46.51	0.913158
DD4	64.27	44.19	4.799525	90.93	18.82	15.94416	52.02	92.76	1.850647
DD8	21.43	26.94	2.625056	15.25	10.07	4.997517	32.12	80.26	1.320658
DD12	82.56	33.99	8.015534	82.56	33.99	8.015534	57.65	91.09	2.088539
DD13	58.65	97.59	1.983246	12.15	12.08	3.319123	54.44	67.62	2.656788

Table S7. Limits of detection determined of each DimerDye for nicotine, MDMA and cocaine in diluted saliva

	Nicotine			MDMA			Cocaine		
	σ	SLOPE	LOD (μM)	σ	SLOPE	LOD (μM)	σ	SLOPE	LOD (μM)
DD1	17.38	2.08	27.57404	30.36	2.428	41.26359	28.54	22.23	4.236707
DD4	134.8	6.003	74.10295	120.8	10.97	36.33911	94.71	41.11	7.602603
DD8	23.88	4.233	18.61658	22.43	3.682	20.10293	45.95	30.63	4.950539
DD12	26.85	5.149	17.2082	26.26	8.699	9.961835	47.81	38.76	4.070511
DD13	52.71	9.283	18.7378	32.75	12.68	8.523265	35.11	43.05	2.691359

10. PCA and LDA analysis

Stocks of each DimerDye (13.4 μM) were prepared in NaH_2PO_4/Na_2HPO_4 (10 mM, pH 7.4) and aliquoted (90 μL) into a 96-well plate to account for 6 replicates of each drug and 2 blanks. This was followed by additions of each drug/buffer (10 μL) to make a final [DD] = 12 μM, [drug] = 100 μM or 0 μM (blank) with a final volume of 100 μL. The fluorescence was measured with $\lambda_{ex.}$ and $\lambda_{em.}$ tabulated below. The raw fluorescence was subtracted from the blank before analysis. The PCA (type: covariance) and LDA analysis (cross-validation) were conducted with XLSTAT and Minitab 18.

Table S8. Excitation and fluorescence emission wavelengths used for each DimerDye

	$\lambda_{ex.}$ (nm)	$\lambda_{em.}$ (nm)
DD1	385	590
DD4	475	570
DD8	375	580
DD12	415	640
DD13	420	635

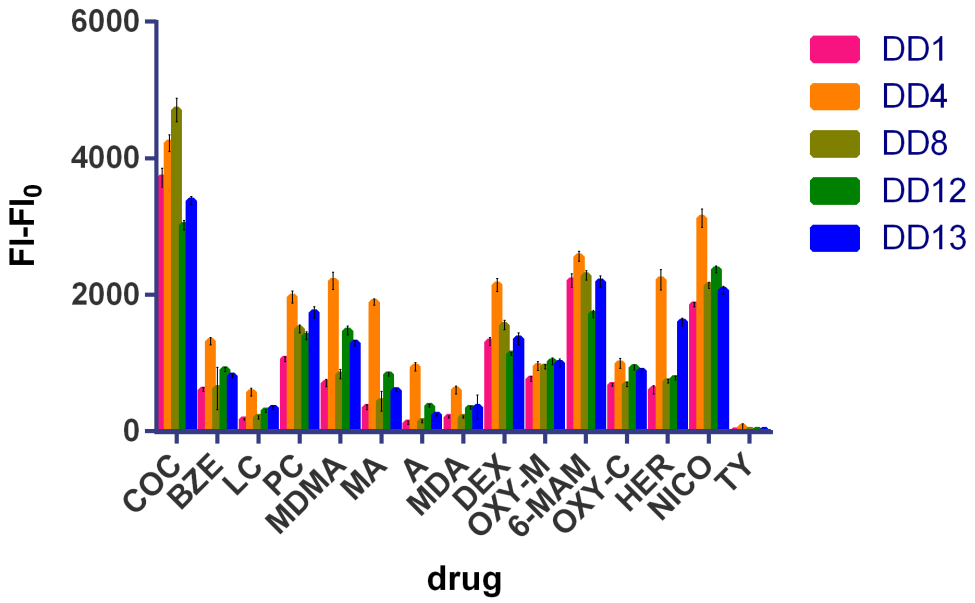

Figure S32. Average fluorescence data from each DD with respect to COC (cocaine), BZE (benzoylecgonine), LC (lidocaine), PC (procaine), MDMA (3,4-methylenedioxymethamphatamine), MA (methamphetamine), A (amphetamine), MDA (3,4-methylenedioxoamphetamine), DEX (dextrorphan), OXY-M (oxymorphone), 6-MAM (6-acetylmorphine), OXY-C (oxycodone), HER (heroin), NICO (nicotine), TY (acetaminophen).

Discriminant Analysis: C7 versus DD1, DD4, DD8, DD12, DD13

Linear Method for Response: C7

Predictors: DD1, DD4, DD8, DD12, DD13

Groups

Group	6-MAM	DEX	HER	OXY-C	OXY-M
Count	6	6	6	6	6

Summary of Classification

	True Group				
Put into Group	6-MAM	DEX	HER	OXY-C	OXY-M
6-MAM	6	0	0	0	0
DEX	0	6	0	0	0
HER	0	0	6	0	0
OXY-C	0	0	0	6	0
OXY-M	0	0	0	0	6
Total N	6	6	6	6	6
N correct	6	6	6	6	6
Proportion	1.000	1.000	1.000	1.000	1.000

Correct Classifications

N	Correct	Proportion
30	30	1.000

Summary of Classification with Cross-validation

	True Group				
Put into Group	6-MAM	DEX	HER	OXY-C	OXY-M
6-MAM	6	0	0	0	0
DEX	0	6	0	0	0
HER	0	0	6	0	0
OXY-C	0	0	0	6	0
OXY-M	0	0	0	0	6
Total N	6	6	6	6	6
N correct	6	6	6	6	6
Proportion	1.000	1.000	1.000	1.000	1.000

Correct Classifications with Cross-validation

N	Correct	Proportion
30	30	1.000

Squared Distance Between Groups

	6-MAM	DEX	HER	OXY-C	OXY-M
6-MAM	0.00	512.96	1700.60	1538.17	1221.73
DEX	512.96	0.00	524.66	390.45	259.67
HER	1700.60	524.66	0.00	278.79	361.25
OXY-C	1538.17	390.45	278.79	0.00	31.07
OXY-M	1221.73	259.67	361.25	31.07	0.00

Linear Discriminant Function for Groups

	6-MAM	DEX	HER	OXY-C	OXY-M
Constant	-2044.5	-925.2	-565.4	-383.1	-480.5
DD1	0.4	0.2	0.0	0.1	0.1
DD4	0.1	0.1	0.2	0.1	0.1
DD8	0.5	0.4	-0.0	0.1	0.2
DD12	0.9	0.6	0.5	0.6	0.6
DD13	0.1	0.0	0.2	0.1	0.1

Summary of Misclassified Observations

					Squared Distance		Probability	
Observation	True Group	Pred Group	X-val Group	Group	Pred	X-val	Pred	X-val

Discriminant Analysis: C10 versus DD1_1, DD4_1, DD8_1, ... 12_1, DD13_1

Linear Method for Response: C10

Predictors: DD1_1, DD4_1, DD8_1, DD12_1, DD13_1

Groups

Group	BZE	COC	LC	PC
Count	6	6	6	6

Summary of Classification

	True Group			
Put into Group	BZE	COC	LC	PC
BZE	6	0	0	0
COC	0	6	0	0
LC	0	0	6	0
PC	0	0	0	6
Total N	6	6	6	6
N correct	6	6	6	6
Proportion	1.000	1.000	1.000	1.000

Correct Classifications

N	Correct	Proportion
24	24	1.000

Summary of Classification with Cross-validation

	True Group			
Put into Group	BZE	COC	LC	PC
BZE	6	0	0	0
COC	0	6	0	0
LC	0	0	6	0
PC	0	0	0	6
Total N	6	6	6	6
N correct	6	6	6	6
Proportion	1.000	1.000	1.000	1.000

Correct Classifications with Cross-validation

N	Correct	Proportion
24	24	1.000

Squared Distance Between Groups

	BZE	COC	LC	PC
BZE	0.00	2751.04	200.06	299.07
COC	2751.04	0.00	4006.46	1520.15
LC	200.06	4006.46	0.00	862.35
PC	299.07	1520.15	862.35	0.00

Linear Discriminant Function for Groups

	BZE	COC	LC	PC
Constant	-261.7	-2462.1	-42.7	-710.5
DD1_1	-0.2	0.0	-0.1	-0.3
DD4_1	0.1	0.1	0.1	0.1
DD8_1	-0.0	-0.0	-0.0	-0.0
DD12_1	0.5	0.8	0.1	0.6
DD13_1	0.1	0.7	0.1	0.4

Summary of Misclassified Observations

					Squared Distance		Probability	
Observation	True Group	Pred Group	X-val Group	Group	Pred	X-val	Pred	X-val

Discriminant Analysis: C18 versus DD1_2, DD4_2, DD8_2, ... _2, DD13_2

Linear Method for Response: C18

Predictors: DD1_2, DD4_2, DD8_2, DD12_2, DD13_2

Groups

Group	A	MA	MDA	MDMA
Count	6	6	6	6

Summary of Classification

	True Group			
Put into Group	A	MA	MDA	MDMA
A	6	0	0	0
MA	0	6	0	0
MDA	0	0	6	0
MDMA	0	0	0	6
Total N	6	6	6	6
N correct	6	6	6	6
Proportion	1.000	1.000	1.000	1.000

Correct Classifications

N	Correct	Proportion
24	24	1.000

Summary of Classification with Cross-validation

	True Group			
Put into Group	A	MA	MDA	MDMA
A	6	0	1	0
MA	0	6	0	0
MDA	0	0	5	0
MDMA	0	0	0	6
Total N	6	6	6	6
N correct	6	6	5	6
Proportion	1.000	1.000	0.833	1.000

Correct Classifications with Cross-validation

N	Correct	Proportion
24	23	0.958

Squared Distance Between Groups

	A	MA	MDA	MDMA
A	0.00	262.02	68.18	984.61
MA	262.02	0.00	468.55	404.44
MDA	68.18	468.55	0.00	1056.58
MDMA	984.61	404.44	1056.58	0.00

Linear Discriminant Function for Groups

	A	MA	MDA	MDMA
Constant	-120.91	-493.59	-60.77	-936.50
DD1_2	-0.27	-0.40	-0.00	-0.12
DD4_2	0.25	0.46	0.10	0.31
DD8_2	0.07	0.15	0.05	0.16
DD12_2	0.04	0.12	0.08	0.58
DD13_2	0.07	0.16	0.06	0.23

Summary of Misclassified Observations

					Squared Distance		Probability	
Observation	True Group	Pred Group	X-val Group	Group	Pred	X-val	Pred	X-val
19**	MDA	MDA	A	A	70.25	286.84	0.00	1.00
				MA	478.81	915.10	0.00	0.00
				MDA	16.30	1020.77	1.00	0.00
				MDMA	1110.96	4313.67	0.00	0.00

(1) Beatty, M. A.; Borges-González, J.; Sinclair, N. J.; Pye, A. T.; Hof, F. Analyte-Driven Disassembly and Turn-On Fluorescent Sensing in Competitive Biological Media. *J. Am. Chem. Soc.* **2018,** *140*, 3500-3504.
(2) Song, X.; Bian, H.; Wang, C.; Hu, M.; Li, N.; Xiao, Y. Development and applications of a near-infrared dye–benzylguanine conjugate to specifically label SNAP-tagged proteins. *Org. Biomol. Chem.* **2017,** *15*, 8091-8101.
(3) Rosania, G. R.; Lee, J. W.; Ding, L.; Yoon, H.-S.; Chang, Y.-T. Combinatorial Approach to Organelle-Targeted Fluorescent Library Based on the Styryl Scaffold. *J. Am. Chem. Soc.* **2003,** *125*, 1130-1131.
(4) Coe, B. J.; Harris, J. A.; Asselberghs, I.; Clays, K.; Olbrechts, G.; Persoons, A.; Hupp, J. T.; Johnson, R. C.; Coles, S. J.; Hursthouse, M. B.; Nakatani, K. Quadratic Nonlinear Optical Properties of N-Aryl Stilbazolium Dyes. *Adv. Funct. Mater.* **2002,** *12*, 110-116.